High-frequency homogenisation in periodic media with imperfect interfaces

Raphaël C Assier, Marie Touboul, Bruno Lombard, Cédric Bellis

High-frequency homogenisation in periodic media with imperfect interfaces

Raphaël C. Assier[a,*], Marie Touboul[b], Bruno Lombard[b], Cédric Bellis[b]

[a]*Department of Mathematics, The University of Manchester, Oxford Road, Manchester, M13 9PL, UK*
[b]*Aix-Marseille Univ, CNRS, Centrale Marseille, LMA, Marseille, France*

Abstract

In this work, the concept of high-frequency homoge- nisation is extended to the case of one-dimensional periodic media with imperfect interfaces of the spring-mass type. In other words, when considering the propagation of elastic waves in such media, displacement and stress discontinuities are allowed across the borders of the periodic cell. As is customary in high-frequency homogenisation, the homogenisation is carried out about the periodic and antiperiodic solutions corresponding to the edges of the Brillouin zone. Comparisons are made with the exact solutions obtained by the Bloch-Floquet approach for the particular examples of monolayered and bilayered materials. Asymptotic approximations are provided for both the higher branches of the dispersion diagram (second-order) and the resulting wave field (leading-order). In these two cases, convergence measurements are carried out to validate the approach. The special case of two branches of the dispersion diagram intersecting with a non-zero slope at an edge of the Brillouin zone (occurrence of a so-called Dirac point) is also considered in detail and illustrated numerically.

Keywords: High-frequency homogenisation, periodic media, imperfect interfaces

1. Introduction

Classically, dynamic homogenisation is understood as a low-frequency approximation to wave propagation in heterogeneous media such as laminates, composites, or more generally any microstructured media. It consists in approximating such media by effective homogeneous media with specific properties. Homogenisation is the mathematical process that allows one to find such properties. Much work on this topic has been carried out since the 1970s and it is not the aim of this introduction to be exhaustive in that regard. A particularly successful approach is the two-scale asymptotic expansion method and the notion of *slow* or *fast* variables (see e.g. [1], [2], [3]). Periodic media, with which we are concerned in this paper, are dealt with very efficiently by such method.

In periodic media, waves can propagate at angular frequencies ω that are not necessarily small. The set of wavenumbers k (also known as Bloch wavenumbers) at which waves propagate

*Corresponding author
Email address: raphael.assier@manchester.ac.uk (Raphaël C. Assier)

depends on the angular frequency through dispersion relations. In particular it can be shown that these dispersion relations can be entirely understood using diagrams restricting the Bloch wavenumbers to lie within the Brillouin zone. In one dimension, when the periodicity of the structure is h say, such Brillouin zone is given by $k \in [0, \pi/h]$. Typically in such problems, the dispersion diagram displays band-gaps, i.e. regions in the angular frequency space where waves cannot propagate. There tends to be infinitely many branches of the dispersion diagram, i.e. for a given Bloch wavenumber, one can find an infinite (countable) set of angular frequencies leading to propagating waves. Again, a lot has been written about this, and we do not aim to give an exhaustive literature review on this point, though we can refer the interested reader to [4] for example. See also [5] for a discussion of the band gaps in periodic materials from a physics point of view.

The idea of *high-frequency homogenisation* is to approximate how the dispersion relation (and hence the media) will behave for angular frequencies ω that are close to the angular frequencies ω_0 corresponding to an edge of the Brillouin zone on the dispersion diagram. In [6], a work that has largely inspired the present paper, Craster et. al. applied a two-scale asymptotic expansion method in order to achieve this for perfect interfaces. Adopting the terminology of [7], we will refer to the homogenisation near the left edge of the Brillouin zone $k \approx 0$ as Finite Frequency Low Wavenumber (FFLW), while the homogenisation near the right edge ($k \approx \pi/h$) will be referred to as Finite Frequency Finite Wavenumber (FFFW). The end result of the high-frequency homogenisation technique is an approximation of the type

$$\text{(FFLW) } \omega^2 = \omega_0^2 + \mathcal{T}(kh)^2 + o\left(\frac{h^2k^2}{L^2}\right) \text{ or (FFFW) } \omega^2 = \omega_0^2 + \mathcal{T}(kh-\pi)^2 + o\left(\frac{h^2\left(\frac{\pi}{h}-k\right)^2}{L^2}\right), \tag{1}$$

where L is a macroscopic characteristic length of the material and the parameter $\mathcal{T} \in \mathbb{R}$ can be determined explicitly. This angular frequency approximation comes together with an associated leading-order approximation to the wave field $U_h(X)$ of the form

$$\text{(FFLW) } U_h(X) = U_h^{(0)}(X) + O\left(\frac{hk}{L}\right) \text{ or (FFFW) } U_h(X) = U_h^{(0)}(X) + O\left(\frac{h}{L}\left(\frac{\pi}{h}-k\right)\right). \tag{2}$$

One should note that in [7], the authors generalised the technique to work in any dimension, and also pushed the asymptotic work one order further than [6]. It is also worth mentioning the more recent work [8], in which the technique was developed while including a source term in the initial evolution equation. As shown in [9], high-frequency homogenisation of wave equations in the time domain can also be carried out, and the methodology has also been applied in a discrete setting to structural mechanics [10] and elastic lattices [11].

In the present work, following the approach of [6], we wish to focus on extending this high-frequency homogenisation technique to one-dimensional periodic media that have an imperfect interface at the edges of the periodic cell, which, to our knowledge, has not been considered before.

Indeed, because of defects like air and cracks or thin layers of glue for example, the contacts between solids are often not perfect, and a jump of the elastic stress and of the elastic displacement can occur across the contact area (the interface). There are different approaches when it comes to modelling such imperfect contact, and we refer to [12] for a comparison between different models. In particular, authors from various disciplines (e.g. non-destructive evaluation of

materials or geophysics), have modelled such situations using the so-called *spring-mass* conditions that we will use in the present work. These conditions, satisfied by wave fields across an interface, are analogous to the mechanical laws of springs [13–16] or springs and masses [17, 18]. Stiffness and mass values are expected to be connected, although not necessarily in a trivial way, to the contact quality [19, 20]. More recently, rational derivations based on asymptotic expansion have been proposed, yielding similar spring-mass models of imperfect interface [21]. For a more in-depth discussion of the modelling of imperfect contact, we kindly refer the reader to our work [22] on low-frequency homogenisation in the time-domain, where both linear and nonlinear imperfect contacts are considered. There exists a significant amount of work considering the homogenisation of such materials in the static regime (see for example [23], [24] and the more recent work [25]) but it seems that dynamic homogenisation has seldom been treated.

The rest of the paper is organised as follows. In §2.1 we formulate the one-dimensional physical problem at hand, namely that of linear elastic wave propagation through a layered material with periodic, possibly space dependent, material properties. The non-dimensionalisation of the problem is performed in §2.2, leading to the introduction of our small parameter δ, which is fully exploited via the two-scale asymptotic expansion method in §2.3. §3.1, §3.2 and §3.3 are respectively dedicated to the asymptotic expansion at order δ^0, δ^1 and δ^2, before combining these results in §3.4 to explicitly obtain the zeroth-order approximated wave-field and the associated formula for the parameter $\mathcal{T}$ introduced in (1). Effectively, §3 provides approximations of both the dispersion diagram (second-order) and the wave-field (first-order) at the edges of the band gaps. In the limiting case of a point on the edge of the Brillouin zone where two branches of the dispersion diagrams intersect with non-zero slope (such intersections are also known in the literature (see e.g. [26], [27] and [7]) as *Dirac points* or *Dirac cones*), the method developed in §3 needs to be adapted. This is what is done in §4, resulting in a linear approximation to the dispersion diagram.

We then illustrate the method on two concrete examples, a homogeneous material (§5.1) and a bilayered material (§5.2) with periodically distributed imperfect interfaces. Such examples are also treated by the Bloch-Floquet analysis (see Appendix A), which allows us to illustrate and quantify the validity of our method. In particular, we discuss the occurrence of Dirac points, for which the approach of §4 should be taken. Perspectives and conclusions are given in §6.

2. Problem formulation

2.1. The physical problem

We consider linear elastic waves propagation at a given angular frequency ω through a periodic medium of periodicity $h > 0$ and with a macroscopic characteristic length $L > 0$. We denote the physical space variable X; the density $\rho_h(X)$ and the Young's modulus $E_h(X)$ of the elastic medium are assumed to be h-periodic piecewise smooth, L^∞ and strictly positive. We may assume without loss of generalities that the edges of the periodic cell are located at $X_n = nh$ for $n \in \mathbb{Z}$, as illustrated in Figure 1 (left). We further assume that the interfaces across the edges of the periodic cells are imperfect, and of the linear spring-mass type, characterised by some mass and stiffness parameters denoted respectively M and K that are both strictly positive. This results in the following governing equation and jump conditions for the displacement field $U_h(X)$:

$$\frac{\mathrm{d}}{\mathrm{d}X}\left(E_h(X)\frac{\mathrm{d}U_h}{\mathrm{d}X}\right) + \rho_h(X)\omega^2 U_h = 0, \text{ with } \begin{cases} [\![U_h]\!]_{X_n} = \frac{1}{K}\left\langle\!\left\langle E_h \frac{\mathrm{d}U_h}{\mathrm{d}X}\right\rangle\!\right\rangle_{X_n}, \\ \left[\!\left[E_h \frac{\mathrm{d}U_h}{\mathrm{d}X}\right]\!\right]_{X_n} = -M\omega^2 \langle\!\langle U_h \rangle\!\rangle_{X_n}, \end{cases} \tag{3}$$

where $[\![\cdot]\!]_{X_n}$ and $\langle\!\langle\cdot\rangle\!\rangle_{X_n}$ are respectively called the jump and mean brackets at the interface X_n, and are defined for any function $g(X)$ by

$$[\![g]\!]_{X_n} = g(X_n^+) - g(X_n^-) \text{ and } \langle\!\langle g\rangle\!\rangle_{X_n} = \frac{1}{2}(g(X_n^+) + g(X_n^-)). \tag{4}$$

Due to the h-periodicity of ρ_h and E_h, it is possible to write them as $\rho_h(X) = \rho\left(\frac{X}{h}\right)$ and $E_h(X) = E\left(\frac{X}{h}\right)$ for some 1-periodic functions ρ and E.

Note 2.1. *Throughout this work, we assume that any discontinuity of ρ and E on $(0,1)$ are of a perfect contact nature. This means that apart from at the interfaces $X = X_n$, we will assume that the displacement $U_h(X)$ and the stress $E_h(X)\frac{\mathrm{d}U_h}{\mathrm{d}X}$ are continuous.*

Classically, such wave propagation problem in periodic media can be understood by using the so-called Bloch-Floquet analysis that consists in seeking solutions of the form

$$U_h(X) = \mathfrak{U}_h(X)e^{ikX},$$

that propagate at the Bloch wavenumber k, and where $\mathfrak{U}_h(X)$ is h-periodic, that is, $\mathfrak{U}_h(X+h) = \mathfrak{U}_h(X)$. In certain simple cases (see e.g. §5.1 and §5.2), this leads to an explicit dispersion relation relating ω to k, the graphical representation of which is the so-called dispersion diagram.

One should note that for $k = 0$, we have $U_h(X) = U_h(X+h)$, i.e. the solution is periodic, while for $k = \frac{\pi}{h}$, we have $U_h(X) = -U_h(X+h)$, i.e. the solution is antiperiodic. Such values of k correspond to the edges of the so-called Brillouin zone. The aim of the present work is to approximate the Bloch-Floquet solutions propagating at wavenumbers that are close to $k = 0$ (FFLW) or $k = \frac{\pi}{h}$ (FFFW) with finite angular frequency $\omega = O(1)$.

2.2. Non-dimensionalisation

In order to simplify the mathematical notations, we start by non-dimensionalising the physical problem (3). In order to do so, we define the characteristic dimensional density $\rho^\star = \langle\rho\rangle$, Young's modulus $E^\star = \langle 1/E\rangle^{-1}$ and wavespeed $c^\star = \sqrt{E^\star/\rho^\star}$, where the average operator $\langle\cdot\rangle$ is defined for any function g as

$$\langle g\rangle = \int_0^1 g(y)\mathrm{d}y. \tag{5}$$

These can be used in order to define the following non-dimensional quantities

$$x = \frac{X}{L},\ \delta = \frac{h}{L},\ \mu = \frac{\omega h}{c^\star},\ \kappa = Lk,\ \alpha = \frac{\rho}{\rho^\star},\ \beta = \frac{E}{E^\star},\ = \frac{Kh}{E^\star},\ = \frac{M}{h\rho^\star},\ u_\delta(x) = \frac{U_h(X)}{L}. \tag{6}$$

The starred quantities $\rho^\star$ and $E^\star$ are chosen for convenience to be the effective properties of the medium obtained by low-frequency homogenisation, implying that $\langle\alpha\rangle = \langle 1/\beta\rangle = 1$, but this choice is somewhat arbitrary. Moreover, we can also show that

$$\rho_h(X) = \rho\left(\frac{X}{h}\right) = \rho\left(\frac{x}{\delta}\right) \text{ and } E_h(X) = E\left(\frac{X}{h}\right) = E\left(\frac{x}{\delta}\right).$$

Using these quantities, (3) can be rewritten as the non-dimensional governing equation

$$\delta^2 \frac{\mathrm{d}}{\mathrm{d}x}\left(\beta\left(\frac{x}{\delta}\right)\frac{\mathrm{d}u_\delta}{\mathrm{d}x}(x)\right) + \mu^2\alpha\left(\frac{x}{\delta}\right)u_\delta(x) = 0, \tag{7}$$

subject to the jump conditions

$$[\![u_\delta]\!]_{x_n} = \frac{\delta}{-}\left\langle\!\!\left\langle \beta\left(\frac{x}{\delta}\right)\frac{\mathrm{d}u_\delta}{\mathrm{d}x}\right\rangle\!\!\right\rangle_{x_n} \text{ and } \delta\left[\!\!\left[\beta\left(\frac{x}{\delta}\right)\frac{\mathrm{d}u_\delta}{\mathrm{d}x}\right]\!\!\right]_{x_n} = -\mu^2\langle\!\langle u_\delta\rangle\!\rangle_{x_n}, \tag{8}$$

in the geometry setting of Figure 1 (centre). The equations (7)-(8) constitute our non-dimensional problem. Note that in this non-dimensional setting, the Bloch-Floquet analysis is still valid, and consists in looking for solutions of the form

$$u_\delta(x) = \mathfrak{u}_\delta(x)e^{i\kappa x}, \tag{9}$$

where κ is the non-dimensional Bloch wavenumber and $\mathfrak{u}_\delta$ is δ-periodic. Note that this implies that u_δ and its derivative u'_δ satisfy

$$u_\delta(x+\delta) = u_\delta(x)e^{i\kappa\delta} \text{ and } u'_\delta(x+\delta) = u'_\delta(x)e^{i\kappa\delta}. \tag{10}$$

Remark 2.1. *The FFLW case corresponds to $\kappa\delta \approx 0$ and the FFFW case corresponds to $\kappa\delta \approx \pi$. When $\kappa\delta$ is exactly 0 (resp. π), then the solution $u_\delta(x)$ is δ-periodic (resp. δ-antiperiodic).*

2.3. Two-scale asymptotic expansion

We will now make the assumption that the macroscopic characteristic length L is much bigger than the periodicity h, implying that $\delta \ll 1$. The material parameters α and β will hence vary on a fine scale associated with the rescaled coordinate $y = x/\delta$ (see Figure 1 (right) for the associated geometrical configuration).

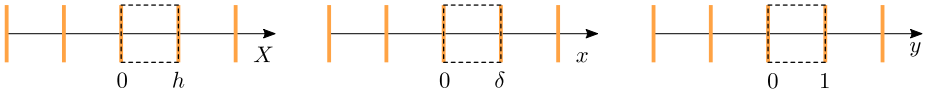

Figure 1: Geometry settings in the X, x and y variables, a periodic cell is highlighted with a dashed line.

Following the two-scale expansion technique, we further assume that the displacement field will have small scale features described by y, and slow continuous variations described by x. We hence pose the following ansatz for the wave field u_δ and the reduced frequency μ:

$$u_\delta(x) = \sum_{j\geqslant 0}\delta^j u_j(x,y) \text{ and } \mu^2 = \sum_{\ell\geqslant 0}\delta^\ell\mu_\ell^2, \tag{11}$$

and treat x and y as two independent variables (scale separation), implying that $\frac{\mathrm{d}}{\mathrm{d}x} \leftrightarrow \frac{\partial}{\partial x} + \frac{1}{\delta}\frac{\partial}{\partial y}$. In the FFLW case we will assume that u_j is 1-periodic in y, that is $u_j(x,y) = u_j(x,y+1)$, while in the FFFW case, we will assume that u_j is 1-antiperiodic, that is $u_j(x,y) = -u_j(x,y+1)$, see Remark 2.1. In what follows, we will attempt to treat both cases simultaneously.

The non-dimensional problem (7)–(8) can hence be rewritten as the governing equation

$$\sum_{j\geqslant 0}\left[\delta^j\frac{\partial}{\partial y}\left(\beta\frac{\partial u_j}{\partial y}\right) + \delta^{j+1}\left\{\beta\frac{\partial^2 u_j}{\partial x\partial y} + \frac{\partial}{\partial y}\left(\beta\frac{\partial u_j}{\partial x}\right)\right\} + \delta^{j+2}\beta\frac{\partial^2 u_j}{\partial x^2} + \sum_{\ell\geqslant 0}\delta^{\ell+j}\mu_\ell^2\alpha u_j\right] = 0, \tag{12}$$

subject to the jump conditions at $y_n = n$:

$$\sum_{j\geqslant 0}\delta^j[\![u_j(x,y)]\!]_{y_n} = \frac{\delta}{-}\sum_{j\geqslant 0}\delta^j\left\langle\!\!\left\langle\beta(y)\left(\frac{\partial u_j}{\partial x}+\frac{1}{\delta}\frac{\partial u_j}{\partial y}\right)\right\rangle\!\!\right\rangle_{y_n}, \tag{13}$$

and

$$\delta\sum_{j\geqslant 0}\delta^j\left[\!\!\left[\beta(y)\left(\frac{\partial u_j}{\partial x}+\frac{1}{\delta}\frac{\partial u_j}{\partial y}\right)\right]\!\!\right]_{y_n} = -\left(\sum_{\ell\geqslant 0}\delta^\ell\mu_\ell^2\right)\left(\sum_{j\geqslant 0}\delta^j\langle\!\langle u_j\rangle\!\rangle_{y_n}\right), \tag{14}$$

where for any function $g(x,y)$, the jump and mean brackets are naturally defined for $n\in\mathbb{Z}$ as

$$[\![g(x,y)]\!]_{y_n} = g(x,n^+) - g(x,n^-) \text{ and } \langle\!\langle g\rangle\!\rangle_{y_n} = \frac{1}{2}(g(x,n^+)+g(x,n^-)). \tag{15}$$

Note 2.2. *In order for our expansion to be compatible with the assumption regarding potential discontinuities of ρ and E within the unit cell made in Note 2.1, we seek the fields such that u_0, $\beta\frac{\partial u_0}{\partial y}$, u_j and $\beta\left(\frac{\partial u_j}{\partial y}+\frac{\partial u_{j-1}}{\partial x}\right)$ for $j\geqslant 1$ are continuous functions of y on $(0,1)$.*

Before pushing the asymptotic analysis further, we need to discuss some important properties of the jump and mean brackets. We will start with a very useful property (that can be proved directly), namely that for any two functions $f(x,y)$ and $g(x,y)$, and any $n\in\mathbb{Z}$, the following relation is valid:

$$[\![fg]\!]_{y_n} = [\![f]\!]_{y_n}\langle\!\langle g\rangle\!\rangle_{y_n} + \langle\!\langle f\rangle\!\rangle_{y_n}[\![g]\!]_{y_n}. \tag{16}$$

It is equally important to note that if the function subjected to the brackets is either periodic or antiperiodic, the following result holds.

Lemma 2.1. *Let $n\in\mathbb{Z}$. If a function $g^{\mathrm{per}}(x,y)$ is 1-periodic in y, then we can write*

$$[\![g^{\mathrm{per}}]\!]_{y_n} = g^{\mathrm{per}}(x,0^+) - g^{\mathrm{per}}(x,1^-) \text{ and } \langle\!\langle g^{\mathrm{per}}\rangle\!\rangle_{y_n} = \frac{1}{2}(g^{\mathrm{per}}(x,0^+)+g^{\mathrm{per}}(x,1^-)),$$

while for a function $g^{\mathrm{anti}}(x,y)$ that is 1-antiperiodic in y, we have

$$[\![g^{\mathrm{anti}}]\!]_{y_n} = g^{\mathrm{anti}}(x,0^+) + g^{\mathrm{anti}}(x,1^-) \text{ and } \langle\!\langle g^{\mathrm{anti}}\rangle\!\rangle_{y_n} = \frac{1}{2}(g^{\mathrm{anti}}(x,0^+)-g^{\mathrm{anti}}(x,1^-)).$$

The Lemma 2.1 means that as long as the function subjected to either the jump or the mean bracket is 1-periodic or 1-antiperiodic in y, then the mean and jump brackets values are independent of n, and the y_n subscript can be dropped. Since $\beta(y)$ is 1-periodic and $u_j(x,y)$ is either 1-periodic or 1-antiperiodic in y, this is the case for all the brackets in the conditions (13) and (14), we will hence drop the subscript from now on and just use $[\![\cdot]\!]$ and $\langle\!\langle\cdot\rangle\!\rangle$. We will make sure that whenever this notation is used, the function inside the brackets is either periodic or antiperiodic. In particular, from Lemma 2.1 and (16), we obtain directly the following lemma that will prove very important in what follows.

Lemma 2.2. *For any two functions $f(x,y)$ and $g(x,y)$ that are either 1-periodic or 1-antiperiodic in y, we have $[\![fg]\!] = [\![f]\!]\langle\!\langle g\rangle\!\rangle + \langle\!\langle f\rangle\!\rangle[\![g]\!]$.*

Finally, in order to efficiently deal with eventual discontinuities of ρ and E (see notes 2.1 and 2.2), and link the average operator and the jump bracket, the following result will be very useful.

Lemma 2.3. *For any function $g^{\mathrm{per}}(x,y)$ that is 1-periodic and piecewise smooth in y, we have*

$$\left\langle \frac{\partial g^{\mathrm{per}}}{\partial y} \right\rangle = -[\![g^{\mathrm{per}}]\!] - J(g^{\mathrm{per}}), \text{ where } J(g^{\mathrm{per}}) = \sum_{q=1}^{Q} (g^{\mathrm{per}}(x, r_q^+) - g^{\mathrm{per}}(x, r_q^-)), \tag{17}$$

where the locations $r_q \in (0,1)$ correspond to potential discontinuities of g^{per}.

Notation 2.1. *From now on, in order to efficiently deal with the FFLW (Finite Frequency Low Wavenumber, $\kappa\delta \approx 0$) and the FFFW (Finite Frequency Finite Wavenumber, $\kappa\delta \approx \pi$) cases simultaneously, we will assume that whenever the symbols $\pm$ or $\mp$ are used, the top sign corresponds to FFLW while the bottom sign corresponds to FFFW.*

We are now well equipped to start developing the core theoretical part of the paper.

3. Asymptotic approximation

We will now deploy the two-scale asymptotic procedure in order to derive the approximation (1). In order to do so we will need to consider the contributions of (12)–(14) at the orders δ^0, δ^1 and δ^2.

3.1. Zeroth-order field

Upon collecting the terms of order δ^0 in (12)–(14), we obtain the system

$$(3.1a)\quad \frac{\partial}{\partial y}\left(\beta \frac{\partial u_0}{\partial y}\right) + \mu_0^2 \alpha u_0 = 0 \quad \text{with} \quad (3.1b)\quad \begin{cases} [\![u_0]\!] = \frac{1}{\pm} \left\langle\!\!\left\langle \beta \frac{\partial u_0}{\partial y} \right\rangle\!\!\right\rangle, \\ \left[\!\!\left[\beta \frac{\partial u_0}{\partial y} \right]\!\!\right] = -\mu_0^2 \langle\!\langle u_0 \rangle\!\rangle. \end{cases} \tag{18}$$

Upon considering the (Sturm-Liouville) differential operator $\mathcal{L} := \frac{-1}{\alpha}\frac{\mathrm{d}}{\mathrm{d}y}\left(\beta \frac{\mathrm{d}}{\mathrm{d}y}\right)$, one can see that the system (18) constitutes an eigenvalue problem for $\mathcal{L}$. It is a bit unusual since the eigenvalue also appears in the boundary conditions, but one can show, using the weighted inner product of $L^2([0,1], \alpha(y)\mathrm{d}y)$ and Lemma 2.2 that this operator is symmetric and self-adjoint in both the FFLW and FFFW cases. Therefore it has a discrete set of real eigenvalues associated to real eigenfunctions. We are here interested in the positive eigenvalues, the square root of which being denoted μ_0. These reduced frequencies μ_0 correspond to the intersection of the dispersion diagram with the left (FFLW) or the right (FFFW) border of the Brillouin zone.

From now on we will choose one of these eigenvalues, denote it by μ_0, and endeavour to approximate the solutions for some parameters (μ, κ) close to $(\mu_0, 0)$ for FFLW or close to $\left(\mu_0, \frac{\pi}{\delta}\right)$ for FFFW. We will also assume that μ_0 is a simple eigenvalue (multiplicity 1). The case of a double eigenvalue will be dealt with in §4. Hence, there is only one eigenfunction that we denote $\hat{u}_0(y)$ and that is either periodic (FFLW) or antiperiodic (FFFW). The associated solution u_0 to (18) can therefore be rewritten

$$u_0(x,y) = \mathcal{U}_0(x)\hat{u}_0(y), \tag{19}$$

for some function $\mathcal{U}_0(x)$. It is worth mentioning at this stage that when inputting (19) into (18), we find that $\hat{u}_0(y)$ satisfies both the equation (18a) and the jump conditions (18b), a fact that will be used throughout the paper.

The main aim of what follows is to derive a differential equation with constant coefficients satisfied by $\mathcal{U}_0(x)$. Note that in the case of low-frequency homogenisation, the zeroth-order field $u_0(x, y)$ can be shown to be independent of y; this is one of the main differences between low- and high-frequency homogenisation.

3.2. First-order field

Let us now set μ_0 to be one of the reduced frequencies found in the previous section, we can collect the terms of order δ^1 in (12)–(14) to obtain the following system governing the first-order field u_1:

$$\frac{\partial}{\partial y}\left(\beta\left(\frac{\partial u_1}{\partial y}+\frac{\partial u_0}{\partial x}\right)\right)+\beta\frac{\partial^2 u_0}{\partial x\partial y}+\alpha(\mu_0^2 u_1+\mu_1^2 u_0)=0, \tag{20}$$

subject to the jump conditions

$$[\![u_1]\!]=\frac{1}{-}\left\langle\!\!\left\langle\beta\left(\frac{\partial u_0}{\partial x}+\frac{\partial u_1}{\partial y}\right)\right\rangle\!\!\right\rangle \text{ and } \left[\!\!\left[\beta\left(\frac{\partial u_0}{\partial x}+\frac{\partial u_1}{\partial y}\right)\right]\!\!\right]=-(\mu_0^2\langle\!\langle u_1\rangle\!\rangle+\mu_1^2\langle\!\langle u_0\rangle\!\rangle). \tag{21}$$

We will show below that there is only one possible value of μ_1, and that it has to be zero.

3.2.1. Proving that $\mu_1 = 0$

Following [6], we consider $\langle u_1\times(18a)-u_0\times(20)\rangle$. The terms in $\alpha\mu_0^2u_0u_1$ cancel out, and we obtain

$$\left\langle u_1\frac{\partial}{\partial y}\left(\beta\frac{\partial u_0}{\partial y}\right)-u_0\frac{\partial}{\partial y}\left(\beta\frac{\partial u_1}{\partial y}\right)\right\rangle=\left\langle\frac{\partial}{\partial y}\left(u_0\beta\frac{\partial u_0}{\partial x}\right)\right\rangle+\underbrace{\left\langle\beta\left(u_0\frac{\partial^2 u_0}{\partial x\partial y}-\frac{\partial u_0}{\partial x}\frac{\partial u_0}{\partial y}\right)\right\rangle}_{=0}+\mu_1^2\langle\alpha u_0^2\rangle. \tag{22}$$

Note that due to the form (19) of u_0, we have $u_0\frac{\partial^2 u_0}{\partial x\partial y}-\frac{\partial u_0}{\partial x}\frac{\partial u_0}{\partial y}=0$, so the second bracket in the RHS of the equation above is actually zero.

By the product rule, the left-hand side (LHS) of (22) can be reduced to

$$\begin{aligned}\left\langle u_1\frac{\partial}{\partial y}\left(\beta\frac{\partial u_0}{\partial y}\right)-u_0\frac{\partial}{\partial y}\left(\beta\frac{\partial u_1}{\partial y}\right)\right\rangle&=\left\langle\frac{\partial}{\partial y}\left(u_1\beta\frac{\partial u_0}{\partial y}\right)\right\rangle-\left\langle\frac{\partial}{\partial y}\left(u_0\beta\frac{\partial u_1}{\partial y}\right)\right\rangle\\&=-\left[\!\!\left[u_1\beta\frac{\partial u_0}{\partial y}\right]\!\!\right]+\left[\!\!\left[u_0\beta\frac{\partial u_1}{\partial y}\right]\!\!\right]+J\left(u_0\beta\frac{\partial u_1}{\partial y}\right),\end{aligned} \tag{23}$$

where we have use the lemmas 2.1 and 2.3, and the facts that both $u_1\beta\frac{\partial u_0}{\partial y}$ and $u_0\beta\frac{\partial u_1}{\partial y}$ are 1-periodic in y and that by Note 2.2, $u_1\beta\frac{\partial u_0}{\partial y}$ is continuous on $(0,1)$. Moreover, by Note 2.2, we know that $u_0\beta\left(\frac{\partial u_1}{\partial y}+\frac{\partial u_0}{\partial x}\right)$ is continuous on $(0,1)$, and hence it transpires that

$$J\left(u_0\beta\frac{\partial u_1}{\partial y}\right)=-J\left(u_0\beta\frac{\partial u_0}{\partial x}\right). \tag{24}$$

We will now focus on the right-hand side (RHS) of (22), using the lemmas 2.1 and 2.3 again, and noting that $u_0\beta\frac{\partial u_0}{\partial x}$ is 1-periodic in y but not necessarily continuous on $(0,1)$, we have

$$\left\langle \frac{\partial}{\partial y}\left(u_0\beta\frac{\partial u_0}{\partial x}\right)\right\rangle = -\left[\!\left[u_0\beta\frac{\partial u_0}{\partial x}\right]\!\right] - J\left(u_0\beta\frac{\partial u_0}{\partial x}\right). \tag{25}$$

Hence, using (23),(24) and (25), we find that the discontinuity terms J disappear, and we can rewrite (22) as

$$\left[\!\left[\beta\left(u_1\frac{\partial u_0}{\partial y} - u_0\frac{\partial u_1}{\partial y}\right)\right]\!\right] = \left[\!\left[u_0\beta\frac{\partial u_0}{\partial x}\right]\!\right] - \mu_1^2\langle\alpha u_0^2\rangle. \tag{26}$$

When perfect interfaces are considered, the jump bracket terms in (26) are automatically zero, a fact that is used in [6] to conclude that $\mu_1 = 0$. Such reasoning cannot be used directly in our case. Instead, we will endeavour to rewrite the LHS of (26) differently by making use of Lemma 2.2, to obtain

$$\left[\!\left[\beta\left(u_1\frac{\partial u_0}{\partial y} - u_0\frac{\partial u_1}{\partial y}\right)\right]\!\right] = [\![u_1]\!]\left\langle\!\left\langle\beta\frac{\partial u_0}{\partial y}\right\rangle\!\right\rangle + \langle\!\langle u_1\rangle\!\rangle\left[\!\left[\beta\frac{\partial u_0}{\partial y}\right]\!\right] - [\![u_0]\!]\left\langle\!\left\langle\beta\frac{\partial u_1}{\partial y}\right\rangle\!\right\rangle - \langle\!\langle u_0\rangle\!\rangle\left[\!\left[\beta\frac{\partial u_1}{\partial y}\right]\!\right]. \tag{27}$$

Using the jump conditions (21), we directly deduce that

$$\left\langle\!\left\langle\beta\frac{\partial u_1}{\partial y}\right\rangle\!\right\rangle = [\![u_1]\!] - \left\langle\!\left\langle\beta\frac{\partial u_0}{\partial x}\right\rangle\!\right\rangle \text{ and } \left[\!\left[\beta\frac{\partial u_1}{\partial y}\right]\!\right] = -(\mu_0^2\langle\!\langle u_1\rangle\!\rangle + \mu_1^2\langle\!\langle u_0\rangle\!\rangle) - \left[\!\left[\beta\frac{\partial u_0}{\partial x}\right]\!\right]. \tag{28}$$

Using (28) and the jump conditions in (18), the RHS of (27) can be simplified to obtain

$$\begin{aligned}\left[\!\left[\beta\left(u_1\frac{\partial u_0}{\partial y} - u_0\frac{\partial u_1}{\partial y}\right)\right]\!\right] &= \left([\![u_0]\!]\left\langle\!\left\langle\beta\frac{\partial u_0}{\partial x}\right\rangle\!\right\rangle + \langle\!\langle u_0\rangle\!\rangle\left[\!\left[\beta\frac{\partial u_0}{\partial x}\right]\!\right]\right) + \mu_1^2\langle\!\langle u_0\rangle\!\rangle^2 \\ &= \left[\!\left[u_0\beta\frac{\partial u_0}{\partial x}\right]\!\right] + \mu_1^2\langle\!\langle u_0\rangle\!\rangle^2,\end{aligned} \tag{29}$$

where the Lemma 2.2 has been used to obtain the last line. Comparing (26) and (29), we obtain

$$\mu_1^2(\langle\alpha u_0^2\rangle + \langle\!\langle u_0\rangle\!\rangle^2) = 0 \text{ implying that } \mu_1 = 0, \tag{30}$$

because and α are strictly positive, and, in the representation (19), $\mathcal{U}_0$ cannot be identically zero and $\hat{u}_0$ is a real function. This result is very important and lies at the heart of the success of the high-frequency homogenisation method.

3.2.2. An expression for $u_1(x,y)$

We can now simplify the equation (20) governing u_1 to

$$\frac{\partial}{\partial y}\left(\beta\frac{\partial u_1}{\partial y}\right) + \alpha\mu_0^2 u_1 = -\mathcal{U}_0'(x)(2\beta(y)\hat{u}_0'(y) + \beta'(y)\hat{u}_0(y)). \tag{31}$$

Upon noting that, because $\hat{u}_0$ is solution to (18a), the field $-y\mathcal{U}_0'(x)\hat{u}_0(y)$ is a particular solution to (31), and that the differential operator applied to u_1 is exactly the same as that of (18a), we can conclude that u_1 can be written as

$$u_1(x,y) = \mathcal{U}_1(x)\hat{u}_0(y) + \mathcal{U}_0'(x)\left(\mathrm{v}_1(y) - y\hat{u}_0(y)\right), \tag{32}$$

for some function $\mathcal{U}_1(x)$ that will be shown not to play any role in what follows, and a function $\mathrm{v}_1(y)$, that is another solution to (18a), independent of $\hat{u}_0(y)$, and that is chosen to ensure that the jump conditions

$$[\![u_1]\!] = \frac{1}{-}\left\langle\!\!\left\langle \beta\left(\frac{\partial u_0}{\partial x} + \frac{\partial u_1}{\partial y}\right)\right\rangle\!\!\right\rangle \text{ and } \left[\!\!\left[\beta\left(\frac{\partial u_0}{\partial x} + \frac{\partial u_1}{\partial y}\right)\right]\!\!\right] = -\mu_0^2\langle\!\langle u_1\rangle\!\rangle \tag{33}$$

are satisfied. These jump conditions come from (21), where we have used that $\mu_1 = 0$. Note that because of (32), and the periodicity properties of u_1 and $\hat{u}_0$, the function $\mathrm{v}_1(y) - y\hat{u}_0(y)$ has to be periodic (FFLW) or antiperiodic (FFFW). Because this function will appear many times in what follows, it is worth giving it a name. Hence, we define

$$f_1(y) \overset{\text{def}}{=} \mathrm{v}_1(y) - y\hat{u}_0(y). \tag{34}$$

Inputting the form (32) into (33), leads to two conditions on f_1:

$$[\![f_1]\!] = \frac{1}{-}\langle\!\langle \beta f_1'\rangle\!\rangle + \frac{1}{-}\langle\!\langle \beta\hat{u}_0\rangle\!\rangle, \tag{35}$$

$$-\mu_0^2\langle\!\langle f_1\rangle\!\rangle = [\![\beta f_1']\!] + [\![\beta\hat{u}_0]\!]. \tag{36}$$

One should notice, in particular, that no terms involving $\mathcal{U}_1(x)$ appear in these conditions.

Remark 3.1. *For practical computations of the function $v_1(y)$, which are required when dealing with specific examples, we can use Lemma 2.1 to rewrite the two jump conditions (35) and (36) as*

$$\mathcal{L}_1[v_1] = \mathcal{K}_1[\hat{u}_0] \text{ and } \mathcal{L}_2[v_1] = \mathcal{K}_2[\hat{u}_0],$$

where

$$\begin{aligned}
\mathcal{L}_1[v_1] &= v_1(0^+) \mp v_1(1^-) - \frac{1}{2}\left(\beta(0^+)v_1'(0^+) \pm \beta(1^-)v_1'(1^-)\right),\\
\mathcal{K}_1[\hat{u}_0] &= \mp\hat{u}_0(1^-) \mp \frac{1}{2}\beta(1^-)\hat{u}_0'(1^-),\\
\mathcal{L}_2[v_1] &= -\frac{\mu_0^2}{2}\left(v_1(0^+) \pm v_1(1^-)\right) - \left(\beta(0^+)v_1'(0^+) \mp \beta(1^-)v_1'(1^-)\right),\\
\mathcal{K}_2[\hat{u}_0] &= \mp\frac{\mu_0^2}{2}\hat{u}_0(1^-) \pm \beta(1^-)\hat{u}_0'(1^-),
\end{aligned}$$

where Notation 2.1 has been used. Note that $\mathcal{L}_{1,2}$ are the same operators as those applied to $\hat{u}_0$ when determining μ_0, though in this case the right-hand side was 0. Here we have these non-zero $\mathcal{K}_{1,2}$ terms.

3.3. Second-order field

We can now collect the terms of order δ^2 in (12)–(14) to obtain the following equation governing the second-order field u_2:

$$\frac{\partial}{\partial y}\left(\beta\frac{\partial u_2}{\partial y}\right) + \mu_0^2\alpha u_2 + \beta\frac{\partial^2 u_1}{\partial x\partial y} + \frac{\partial}{\partial y}\left(\beta\frac{\partial u_1}{\partial x}\right) + \beta\frac{\partial^2 u_0}{\partial x^2} + \mu_2^2\alpha u_0 = 0, \tag{37}$$

subject to the jump conditions

$$[\![u_2]\!] = \frac{1}{-}\left\langle\!\!\left\langle \beta\left(\frac{\partial u_2}{\partial y} + \frac{\partial u_1}{\partial x}\right)\right\rangle\!\!\right\rangle \text{ and } \left[\!\!\left[\beta\left(\frac{\partial u_2}{\partial y} + \frac{\partial u_1}{\partial x}\right)\right]\!\!\right] = -(\mu_0^2 \langle\!\langle u_2 \rangle\!\rangle + \mu_2^2 \langle\!\langle u_0 \rangle\!\rangle). \tag{38}$$

Similarly to §3.2.1(b), we consider the quantity $\langle u_2 \times (18a) - u_0 \times (37)\rangle$. The terms in $\alpha\mu_0^2 u_0 u_2$ cancel out, and, using the representation (19), and dividing through by $\mathcal{U}_0(x)$, we obtain

$$\left\langle u_2 \frac{\mathrm{d}}{\mathrm{d}y}\left(\beta\frac{\mathrm{d}\hat{u}_0}{\mathrm{d}y}\right) - \hat{u}_0\frac{\partial}{\partial y}\left(\beta\frac{\partial u_2}{\partial y}\right)\right\rangle = \left\langle \hat{u}_0\beta\frac{\partial^2 u_1}{\partial x \partial y} + \hat{u}_0\frac{\partial}{\partial y}\left(\beta\frac{\partial u_1}{\partial x}\right)\right\rangle + \mathcal{U}_0''(x)\langle\beta(\hat{u}_0)^2\rangle + \mu_2^2\langle\alpha(\hat{u}_0)^2\rangle\mathcal{U}_0(x). \tag{39}$$

3.3.1. A first manipulation

As in §3.2.1(b), the term on the LHS of (39) can be simplified using the product rule, Lemma 2.1, Note 2.2 and Lemma 2.3, to obtain

$$\left\langle u_2 \frac{\mathrm{d}}{\mathrm{d}y}\left(\beta\frac{\mathrm{d}\hat{u}_0}{\mathrm{d}y}\right) - \hat{u}_0\frac{\partial}{\partial y}\left(\beta\frac{\partial u_2}{\partial y}\right)\right\rangle = -\left[\!\!\left[u_2\beta\frac{\mathrm{d}\hat{u}_0}{\mathrm{d}y}\right]\!\!\right] + \left[\!\!\left[\hat{u}_0\beta\frac{\partial u_2}{\partial y}\right]\!\!\right] + J\left(\hat{u}_0\beta\frac{\partial u_2}{\partial y}\right), \tag{40}$$

and it can be shown that

$$J\left(\hat{u}_0\beta\frac{\partial u_2}{\partial y}\right) = -J\left(\hat{u}_0\beta\frac{\partial u_1}{\partial x}\right) = -\mathcal{U}_1'(x)J(\beta(\hat{u}_0)^2) - \mathcal{U}_0''(x)J(\hat{u}_0\beta f_1). \tag{41}$$

Focusing now on the RHS of (39) and using (32) directly, we get

$$\hat{u}_0\beta\frac{\partial^2 u_1}{\partial x\partial y} = \mathcal{U}_1'(x)\beta\hat{u}_0\hat{u}_0' + \mathcal{U}_0''(x)\beta\hat{u}_0 f_1' \text{ and } \hat{u}_0\frac{\partial}{\partial y}\left(\beta\frac{\partial u_1}{\partial x}\right) = \mathcal{U}_1'(x)\hat{u}_0(\beta\hat{u}_0)' + \mathcal{U}_0''(x)\hat{u}_0(\beta f_1)',$$

which, with little algebraic manipulation, implies that

$$\left\langle \hat{u}_0\beta\frac{\partial^2 u_1}{\partial x\partial y} + \hat{u}_0\frac{\partial}{\partial y}\left(\beta\frac{\partial u_1}{\partial y}\right)\right\rangle = \mathcal{U}_1'(x)\langle(\beta(\hat{u}_0)^2)'\rangle + \mathcal{U}_0''(x)\langle(\beta\hat{u}_0 f_1)'\rangle + \mathcal{U}_0''(x)\langle\beta(\hat{u}_0 f_1' - \hat{u}_0' f_1)\rangle. \tag{42}$$

Because $\hat{u}_0$ and f_1 have the same periodicity property, and β is periodic, the functions $\beta\hat{u}_0 f_1$ and $\beta(\hat{u}_0)^2$ are periodic (in both the FFLW and FFFW cases), but note that they are not necessarily continuous on $(0, 1)$. Hence, we can use Lemma 2.3, to have

$$\langle(\beta(\hat{u}_0)^2)'\rangle = -[\![\beta(\hat{u}_0)^2]\!] - J(\beta(\hat{u}_0)^2) \text{ and } \langle(\beta\hat{u}_0 f_1)'\rangle = -[\![\beta\hat{u}_0 f_1]\!] - J(\beta\hat{u}_0 f_1). \tag{43}$$

Finally, upon defining

$$w_1 \overset{\text{def}}{=} \hat{u}_0 f_1' - \hat{u}_0' f_1 + (\hat{u}_0)^2, \tag{44}$$

and using (40), (41), (42) and (44), we can rewrite (39) as

$$\left[\!\!\left[\beta\left(u_2\frac{\mathrm{d}\hat{u}_0}{\mathrm{d}y} - \hat{u}_0\frac{\partial u_2}{\partial y}\right)\right]\!\!\right] = \mathcal{U}_1'(x)[\![\beta(\hat{u}_0)^2]\!] + \mathcal{U}_0''(x)[\![\beta\hat{u}_0 f_1]\!] - \mathcal{U}_0''(x)\langle\beta w_1\rangle - \mu_2^2\langle\alpha(\hat{u}_0)^2\rangle\mathcal{U}_0(x). \tag{45}$$

Remark 3.2. *Inputting (34) into (44), one shows that* $w_1 = \hat{u}_0 v_1' - \hat{u}_0' v_1$*, which is the Wronskian associated to the second-order ODE* $(\beta g')' + \mu_0^2 \alpha g = 0$*, and hence satisfies the first-order ODE* $(\beta w_1)' = 0$*. Moreover, the hypothesis made in Note 2.2 regarding potential material properties discontinuities within the interior of the unit cell implies that* $\hat{u}_0$*,* $\beta\hat{u}_0'$*,* u_1 *and* $\beta\left(\frac{\partial u_1}{\partial y} + \mathcal{U}_0'(x)\hat{u}_0\right)$ *are continuous in* y *on* $(0,1)$*. Using the form (32) of* u_1*, this implies that both* v_1 *and* $\beta v_1'$ *should be continuous on* $(0,1)$*, and hence that* βw_1 *is continuous on* $(0,1)$*, which, using the fact that* $(\beta w_1)' = 0$*, implies that* βw_1 *is constant on* $(0,1)$*. Therefore* $\langle \beta w_1 \rangle = \beta(0^+) w_1(0^+)$ *say, and its computation does not require any integration. Moreover, since* $\hat{u}_0$ *and* v_1 *are independent, it is clear that* $\langle \beta w_1 \rangle \neq 0$*.*

3.3.2. A second manipulation

In a second step, we can evaluate the LHS of (45) directly by making use of Lemma 2.2 to obtain

$$\left[\!\!\left[\beta\left(u_2\frac{\mathrm{d}\hat{u}_0}{\mathrm{d}y} - \hat{u}_0\frac{\partial u_2}{\partial y}\right)\right]\!\!\right] = [\![u_2]\!]\langle\!\langle\beta\hat{u}_0'\rangle\!\rangle + \langle\!\langle u_2\rangle\!\rangle[\![\beta\hat{u}_0']\!] - [\![\hat{u}_0]\!]\left\langle\!\!\left\langle\beta\frac{\partial u_2}{\partial y}\right\rangle\!\!\right\rangle - \langle\!\langle\hat{u}_0\rangle\!\rangle\left[\!\!\left[\beta\frac{\partial u_2}{\partial y}\right]\!\!\right]. \quad (46)$$

Using (32), (34) and the jump conditions (38), we find that

$$\left\langle\!\!\left\langle\beta\frac{\partial u_2}{\partial y}\right\rangle\!\!\right\rangle = [\![u_2]\!] - \mathcal{U}_1'(x)\langle\!\langle\beta\hat{u}_0\rangle\!\rangle - \mathcal{U}_0''(x)\langle\!\langle\beta f_1\rangle\!\rangle,$$
$$\left[\!\!\left[\beta\frac{\partial u_2}{\partial y}\right]\!\!\right] = -(\mu_0^2\langle\!\langle u_2\rangle\!\rangle + \mu_2^2\mathcal{U}_0(x)\langle\!\langle\hat{u}_0\rangle\!\rangle) - \mathcal{U}_1'(x)[\![\beta\hat{u}_0]\!] - \mathcal{U}_0''(x)[\![\beta f_1]\!].$$

We can hence use this and the jump conditions of (18), and notice that the terms in and μ_0^2 cancel out, to rewrite (46) as

$$\left[\!\!\left[\beta\left(u_2\frac{\mathrm{d}\hat{u}_0}{\mathrm{d}y} - \hat{u}_0\frac{\partial u_2}{\partial y}\right)\right]\!\!\right] = \mathcal{U}_1'(x)([\![\hat{u}_0]\!]\langle\!\langle\beta\hat{u}_0\rangle\!\rangle + \langle\!\langle\hat{u}_0\rangle\!\rangle[\![\beta\hat{u}_0]\!]) + \mathcal{U}_0''(x)([\![\hat{u}_0]\!]\langle\!\langle\beta f_1\rangle\!\rangle + \langle\!\langle\hat{u}_0\rangle\!\rangle[\![\beta f_1]\!])$$
$$+ \mu_2^2\mathcal{U}_0(x)\langle\!\langle\hat{u}_0\rangle\!\rangle^2, \quad (47)$$

which, using Lemma 2.2, simplifies to

$$\left[\!\!\left[\beta\left(u_2\frac{\mathrm{d}\hat{u}_0}{\mathrm{d}y} - \hat{u}_0\frac{\partial u_2}{\partial y}\right)\right]\!\!\right] = \mathcal{U}_1'(x)[\![\beta(\hat{u}_0)^2]\!] + \mathcal{U}_0''(x)[\![\beta\hat{u}_0 f_1]\!] + \mu_2^2\mathcal{U}_0(x)\langle\!\langle\hat{u}_0\rangle\!\rangle^2. \quad (48)$$

3.4. The effective equation for $\mathcal{U}_0$ *and dispersion branches approximation*

We can now equate (45) and (48) and note that the terms involving $\mathcal{U}_1'$ and $[\![\beta\hat{u}_0 f_1]\!]$ cancel out, to conclude that

$$T\mathcal{U}_0''(x) + \mu_2^2\mathcal{U}_0(x) = 0, \text{ where } T = \frac{\langle\beta w_1\rangle}{\langle\alpha(\hat{u}_0)^2\rangle + \langle\!\langle\hat{u}_0\rangle\!\rangle^2}. \quad (49)$$

Note that $T \neq 0$, but it can be either negative or positive. Since we are looking for standing waves, we seek μ_2^2 such that $\mu_2^2/T \geqslant 0$. Remember that μ_2 is a correction term to the reduced frequency μ, such that $\mu^2 = \mu_0^2 + \delta^2\mu_2^2 + o(\delta^2)$. This means that for each branch of the dispersion diagram (determined by our initial choice of eigenvalue μ_0), we look for a function $\mu_2(\kappa)$ that

will lead to an approximation of $\mu(\kappa)$ at the second order in δ, where κ is the reduced Bloch wavenumber. In particular, by definition of the FFLW and FFFW cases, we should have

$$\text{(FFLW)}\ \ \mu_2(\kappa) \underset{\kappa\to 0}{\to} 0 \ \text{ and } \ \text{(FFFW)}\ \ \mu_2(\kappa) \underset{\kappa\to \frac{\pi}{\delta}}{\to} 0. \tag{50}$$

In order for our asymptotic representation (11) to be compatible with the fact that u_δ should satisfy the Bloch-Floquet conditions (10), it is enough to impose that all the $u_j\left(x, \frac{x}{\delta}\right)$ should also satisfy these conditions. For $j = 0$, this means that

$$\mathcal{U}_0(x+\delta)\hat{u}_0\left(\frac{x}{\delta}+1\right) = \mathcal{U}_0(x)\hat{u}_0\left(\frac{x}{\delta}\right)e^{i\kappa\delta}. \tag{51}$$

Hence, due to fact that $\hat{u}_0$ is periodic (FFLW) or antiperiodic (FFFW), we can cancel out the terms in $\hat{u}_0$ in (51) to get

$$\mathcal{U}_0(x+\delta) = \pm\mathcal{U}_0(x)e^{i\kappa\delta}, \tag{52}$$

where, in (52) and below, Notation 2.1 is being used. The second Bloch-Floquet condition in (10), combined with (52), implies that

$$\mathcal{U}_0'(x+\delta) = \pm\mathcal{U}_0'(x)e^{i\kappa\delta}. \tag{53}$$

Because $\mathcal{U}_0$ is solution to (49), it can be written $\mathcal{U}_0(x) = Ae^{i\sqrt{\mu_2^2/T}x} + Be^{-i\sqrt{\mu_2^2/T}x}$ for some constants A and B. The Bloch-Floquet conditions (52) and (53) lead to

$$A\left(1 \mp e^{i\delta\left(\sqrt{\mu_2^2/T}-\kappa\right)}\right) = 0 \ \text{ and } \ B\left(1 \mp e^{-i\delta\left(\sqrt{\mu_2^2/T}+\kappa\right)}\right) = 0. \tag{54}$$

Since κ is restricted to $\left(0, \frac{\pi}{\delta}\right)$, i.e. to the first Brillouin zone in the dispersion diagram, and since it is assumed that $\mu_2^2/T \geqslant 0$, (54) implies that we have

$$\begin{aligned}
&\text{(FFLW)} \quad : \quad \sqrt{\mu_2^2/T} = \kappa, \qquad B = 0, \quad \mathcal{U}_0(x) = e^{i\kappa x},\\
&\text{(FFFW)} \quad : \quad \sqrt{\mu_2^2/T} = \tfrac{\pi}{\delta} - \kappa, \quad A = 0, \quad \mathcal{U}_0(x) = e^{i(\kappa-\frac{\pi}{\delta})x},
\end{aligned}$$

which gives the following approximation for the reduced frequency $\mu(\kappa)$

$$\text{(FFLW)}\ \ \mu^2 = \mu_0^2 + T(\kappa\delta)^2 + o(\kappa^2\delta^2), \ \ \text{(FFFW)}\ \ \mu^2 = \mu_0^2 + T(\kappa\delta-\pi)^2 + o\left(\delta^2\left(\frac{\pi}{\delta}-\kappa\right)^2\right), \tag{55}$$

or, equivalently,

$$\text{(FFLW)}\ \ \mu = \mu_0 + \frac{T}{2\mu_0}(\kappa\delta)^2 + o(\kappa^2\delta^2), \ \ \text{(FFFW)}\ \ \mu = \mu_0 + \frac{T}{2\mu_0}(\kappa\delta-\pi)^2 + o\left(\delta^2\left(\frac{\pi}{\delta}-\kappa\right)^2\right). \tag{56}$$

The non-dimensional wave field is approximated by

$$u_\delta(x) = \underbrace{\mathcal{U}_0(x)\hat{u}_0(x/\delta)}_{u_0(x,x/\delta)} + \begin{cases} O(\kappa\delta) & \text{(FFLW)},\\ O\left(\left(\frac{\pi}{\delta}-\kappa\right)\delta\right) & \text{(FFFW)}. \end{cases} \tag{57}$$

Note that in §5, we will find it more convenient to test the validity of (57) when it is written in terms of the variable y as follows

$$u_\delta(\delta y) = \underbrace{\mathcal{U}_0(\delta y)\hat{u}_0(y)}_{u_0(\delta y, y)} + \begin{cases} O(\kappa\delta) & \text{(FFLW)}, \\ O\left(\left(\frac{\pi}{\delta} - \kappa\right)\delta\right) & \text{(FFFW)}. \end{cases} \tag{58}$$

Hence, as anticipated, using (6), our results can be summarised in dimensional form by (1) and (2), where the parameter $\mathcal{T}$ and the leading-order wave field $U_h^{(0)}$ are given by

$$\mathcal{T} = \frac{(c^\star)^2}{h^2}T, \ \omega_0 = \frac{c^\star \mu_0}{h} \ \text{ and } \ U_h^{(0)}(X) = \begin{cases} e^{ikX}\hat{u}_0(X/h) & \text{(FFLW)}, \\ e^{i(k-\frac{\pi}{h})X}\hat{u}_0(X/h) & \text{(FFFW)}. \end{cases}$$

4. The case of a double eigenvalue μ_0

4.1. A new form for u_0

In order to write (19), we assumed that μ_0 was a simple eigenvalue. If instead we assume that μ_0 has multiplicity 2 say, then we write

$$u_0(x,y) = \underbrace{\mathcal{U}_0^{(1)}(x)\hat{u}_0^{(1)}(y)}_{u_0^{(1)}(x,y)} + \underbrace{\mathcal{U}_0^{(2)}(x)\hat{u}_0^{(2)}(y)}_{u_0^{(2)}(x,y)}, \tag{59}$$

where $\hat{u}_0^{(1)}(y)$ and $\hat{u}_0^{(2)}(y)$ are two independent eigenfunctions associated to the double eigenvalue μ_0 and $\mathcal{U}_0^{(1)}(x)$ and $\mathcal{U}_0^{(2)}(x)$ are some functions of x to be determined.

4.2. In this case, we cannot conclude that $\mu_1 = 0$

We will now apply the same methodology as in §3.2.1(b). In fact the important equations (22), (23) and (29) remain valid. The only difference is that because of the form (59) of u_0, we do not have $u_0\frac{\partial^2 u_0}{\partial x \partial y} - \frac{\partial u_0}{\partial x}\frac{\partial u_0}{\partial y} = 0$ anymore in (22). Instead it can be shown that

$$u_0\frac{\partial^2 u_0}{\partial x \partial y} - \frac{\partial u_0}{\partial x}\frac{\partial u_0}{\partial y} = \mathcal{W}_0(x)\mathtt{w}_0(y), \tag{60}$$

where

$$\mathtt{w}_0(y) = \hat{u}_0^{(1)}(y)\hat{u}_0^{(2)\prime}(y) - \hat{u}_0^{(1)\prime}(y)\hat{u}_0^{(2)}(y) \ \text{ and } \ \mathcal{W}_0(x) = \mathcal{U}_0^{(1)}(x)\mathcal{U}_0^{(2)\prime}(x) - \mathcal{U}_0^{(2)}(x)\mathcal{U}_0^{(1)\prime}(x). \tag{61}$$

Hence the equation (26) will have an extra term and should read

$$\left[\!\!\left[\beta\left(u_1\frac{\partial u_0}{\partial y} - u_0\frac{\partial u_1}{\partial y}\right)\right]\!\!\right] = \left[\!\!\left[u_0\beta\frac{\partial u_0}{\partial x}\right]\!\!\right] - \mathcal{W}_0(x)\,\langle\beta\mathtt{w}_0\rangle - \mu_1^2\langle\alpha u_0^2\rangle. \tag{62}$$

As a result, comparing (62) and (29), we obtain the double eigenvalue equivalent of (30):

$$\mathcal{W}_0(x)\,\langle\beta\mathtt{w}_0\rangle + \mu_1^2(\langle\alpha u_0^2\rangle + \langle\!\langle u_0\rangle\!\rangle^2) = 0, \tag{63}$$

and, in this case, we cannot conclude that $\mu_1 = 0$. Note that $\mathtt{w}_0$ is the Wronskian determinant associated to (18a), and $\beta\mathtt{w}_0$ can be shown to be continuous on the unit cell, hence we conclude that $\beta\mathtt{w}_0$ is actually constant, and hence we can see that $\langle\beta\mathtt{w}_0\rangle = \beta(0^+)\mathtt{w}_0(0^+)$.

4.3. Solving a first-order ODE system to obtain μ_1

Let us note that, using the form (59), we can write

$$\langle\!\langle u_0 \rangle\!\rangle^2 = \mathcal{U}_0^{(1)}(x)\{B_1^2\mathcal{U}_0^{(1)}(x) + B_1B_2\mathcal{U}_0^{(2)}(x)\} + \mathcal{U}_0^{(2)}(x)\{B_2^2\mathcal{U}_0^{(2)}(x) + B_1B_2\mathcal{U}_0^{(1)}(x)\}, \tag{64}$$

$$\langle \alpha u_0^2 \rangle = \mathcal{U}_0^{(1)}(x)\{C_1\mathcal{U}_0^{(1)}(x) + D\mathcal{U}_0^{(2)}(x)\} + \mathcal{U}_0^{(2)}(x)\{C_2\mathcal{U}_0^{(2)}(x) + D\mathcal{U}_0^{(1)}(x)\}, \tag{65}$$

where

$$B_1 = \langle\!\langle \hat{u}_0^{(1)} \rangle\!\rangle,\ B_2 = \langle\!\langle \hat{u}_0^{(2)} \rangle\!\rangle,\ C_1 = \langle \alpha(\hat{u}_0^{(1)})^2 \rangle,\ C_2 = \langle \alpha(\hat{u}_0^{(2)})^2 \rangle,\ D = \langle \alpha \hat{u}_0^{(1)} \hat{u}_0^{(2)} \rangle.$$

Inputting the definition (61) and (64)–(65) into (63), we obtain

$$\begin{aligned} &\mathcal{U}_0^{(1)}(x)\left\{\mathcal{U}_0^{(2)\prime}(x) + \frac{\mu_1^2}{\langle \beta \mathtt{w}_0 \rangle}([B_1^2 + C_1]\mathcal{U}_0^{(1)}(x) + [B_1B_2 + D]\mathcal{U}_0^{(2)}(x))\right\} \\ &-\mathcal{U}_0^{(2)}(x)\left\{\mathcal{U}_0^{(1)\prime}(x) - \frac{\mu_1^2}{\langle \beta \mathtt{w}_0 \rangle}([B_1B_2 + D]\mathcal{U}_0^{(1)}(x) + [B_2^2 + C_2]\mathcal{U}_0^{(2)}(x))\right\} = 0, \end{aligned} \tag{66}$$

which can be rewritten more succinctly as

$$\boldsymbol{\mathcal{U}} \times \left(\boldsymbol{\mathcal{U}}' - \frac{\mu_1^2}{\langle \beta \mathtt{w}_0 \rangle}\mathcal{N}\boldsymbol{\mathcal{U}}\right) = 0 \ \text{ where } \ \mathcal{N} = \begin{pmatrix} B_1B_2 + D & B_2^2 + C_2 \\ -(B_1^2 + C_1) & -(B_1B_2 + D) \end{pmatrix}, \tag{67}$$

and $\boldsymbol{\mathcal{U}} = (\mathcal{U}_0^{(1)}, \mathcal{U}_0^{(2)})^T$. This therefore leads to several possible solution. We could have $\boldsymbol{\mathcal{U}} = \mathbf{0}$, which of course is discarded or we could have $\boldsymbol{\mathcal{U}}' - \frac{\mu_1^2}{\langle \beta \mathtt{w}_0 \rangle}\mathcal{N}\boldsymbol{\mathcal{U}} = a\boldsymbol{\mathcal{U}}$ for some $a \in \mathbb{C}$. If one assumes that $a \neq 0$, a reasoning very similar to the one below will lead to the fact that: if $a \notin i\mathbb{R}$, then the solution obtained will be either exponentially decaying or exponentially growing, and does not correspond to a propagating wave. If $a \in i\mathbb{R}$, we find that the two slopes emerging from a Dirac point will not be opposite of each other, which would lead to a non-smooth dispersion relation (and to an inability to define a group velocity uniquely at this point) and hence this case should also be discarded.

The only possible choice of a is hence $a = 0$. This leads to two coupled ODEs that can be written in matrix form as

$$\boldsymbol{\mathcal{U}}'(x) = \frac{\mu_1^2}{\langle \beta \mathtt{w}_0 \rangle}\mathcal{N}\boldsymbol{\mathcal{U}}(x). \tag{68}$$

The two eigenvalues $\lambda_{1,2}$ of $\mathcal{N}$ are given by

$$\lambda_j = i(-1)^j \sqrt{(B_1^2 + C_1)(B_2^2 + C_2) - (B_1B_2 + D)^2}, \tag{69}$$

as it can be shown, using Cauchy-Schwarz inequality, that the quantity inside the square root is positive. The associated eigenvectors are given by

$$\boldsymbol{\mathcal{U}}_{\lambda_j} = \left(\frac{-(B_1B_2 + D) - \lambda_j}{B_1^2 + C_1}, 1\right)^T, \tag{70}$$

and hence, upon introducing T_d to be

$$T_d = \langle \beta \mathtt{w}_0 \rangle \,/\, \sqrt{(B_1^2 + C_1)(B_2^2 + C_2) - (B_1B_2 + D)^2},$$

the solution to (68) can be written as

$$\boldsymbol{\mathcal{U}}(x) = \mathfrak{c}_1 \boldsymbol{\mathcal{U}}_{\lambda_1} e^{\frac{\mu_1^2}{\langle \beta u_0 \rangle} \lambda_1 x} + \mathfrak{c}_2 \boldsymbol{\mathcal{U}}_{\lambda_2} e^{\frac{\mu_1^2}{\langle \beta u_0 \rangle} \lambda_2 x} = \mathfrak{c}_1 \boldsymbol{\mathcal{U}}_{\lambda_1} e^{-i \frac{\mu_1^2}{T_d} x} + \mathfrak{c}_2 \boldsymbol{\mathcal{U}}_{\lambda_2} e^{i \frac{\mu_1^2}{T_d} x}, \tag{71}$$

for some constants $\mathfrak{c}_{1,2}$. At this stage, we need to remember the Bloch-Floquet conditions (10), which, when applied to u_0 imply that

$$\hat{u}_0^{(1)}(y)\{\pm \mathcal{U}_0^{(1)}(x+\delta) - e^{i\kappa\delta} \mathcal{U}_0^{(1)}(x)\} + \hat{u}_0^{(2)}(y)\{\pm \mathcal{U}_0^{(2)}(x+\delta) - e^{i\kappa\delta} \mathcal{U}_0^{(2)}(x)\} = 0,$$

where Notation 2.1 has been used. Since $\hat{u}_0^{(1)}$ and $\hat{u}_0^{(2)}$ are linearly independent, this implies that $\pm \boldsymbol{\mathcal{U}}(x+\delta) = e^{i\kappa\delta} \boldsymbol{\mathcal{U}}(x)$. Applying this condition to (71), leads to the value of μ_1^2 as follows

$$\text{FFLW} : \left\{ \begin{array}{c} \left\{ \begin{array}{c} \delta\mu_1^2 = -T_d \kappa\delta, \\ \mathfrak{c}_2 = 0, \end{array} \right. \\ \text{or} \\ \left\{ \begin{array}{c} \mathfrak{c}_1 = 0, \\ \delta\mu_1^2 = +T_d \kappa\delta, \end{array} \right. \end{array} \right. \quad \text{and} \quad \text{FFFW} : \left\{ \begin{array}{c} \left\{ \begin{array}{c} \delta\mu_1^2 = +T_d(\pi - \kappa\delta), \\ \mathfrak{c}_2 = 0, \end{array} \right. \\ \text{or} \\ \left\{ \begin{array}{c} \mathfrak{c}_1 = 0, \\ \delta\mu_1^2 = -T_d(\pi - \kappa\delta). \end{array} \right. \end{array} \right. \tag{72}$$

Note that, with (72) we have shown that $\mathcal{U}_0^{(1)}(x)$ and $\mathcal{U}_0^{(2)}(x)$ are proportional. Hence we can conclude that $\mathcal{W}_0(x) \equiv 0$. This may seem surprising since the relation (63) now becomes

$$\mu_1^2(\langle \alpha u_0^2 \rangle + \langle\!\langle u_0 \rangle\!\rangle^2) = 0,$$

and one would be tempted to conclude, as we did in §3.2.1(b), that $\mu_1 = 0$, which would be a contradiction. However, using the form (70) of the eigenvectors, one can show, in the four cases of (72), that we actually have

$$\langle \alpha u_0^2 \rangle + \langle\!\langle u_0 \rangle\!\rangle^2 = 0,$$

and hence no contradiction occurs.

Hence, since $\mu^2 = \mu_0^2 + \delta\mu_1^2 + o(\delta)$, we obtain the linear approximations

$$(\text{FFLW}) : \mu = \mu_0 \pm \frac{T_d}{2\mu_0}(\kappa\delta) + o(\kappa\delta) \quad \text{and} \quad (\text{FFFW}) : \mu = \mu_0 \pm \frac{T_d}{2\mu_0}(\pi - \kappa\delta) + o\left(\left(\frac{\pi}{\delta} - \kappa\right)\delta\right). \tag{73}$$

Here, the symbol ± should not be understood as per Notation 2.1, but as two different slopes, so that, near each double eigenvalue μ_0 of the dispersion diagram, we have two linear approximations with opposite slopes emerging from μ_0. Such behaviour of the dispersion diagram, is that of so-called Dirac points.

5. Examples and numerical experiments

The theory developed above has the advantage to be valid for any spatially varying periodic material properties, even in cases when the dispersion diagram cannot be obtained analytically or is computationally intricate to obtain. However, in order to validate the method, we now consider two simpler examples, for which the dispersion diagram can be obtained directly by the Bloch-Floquet analysis.

5.1. Monolayer

The simplest example that can be considered is the case of a monolayer material with imperfect interface. By this we mean that the density and Young's modulus are constant, so that $\rho_h(X) = \rho^\star$ and $E_h(X) = E^\star$. This implies that $\alpha = \beta = 1$. The geometry of the physical problem is represented in Figure 2.

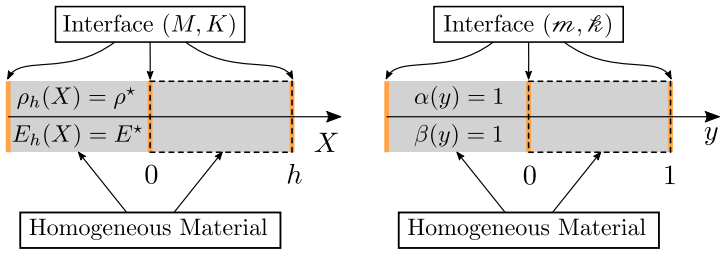

Figure 2: Geometry of the monolayer problem in the physical (left) and nondimensional (right) settings.

The Bloch-Floquet analysis (see Appendix A) gives the following dispersion relation

$$\cos(\kappa\delta) = \frac{1}{1+\frac{\mu^2}{4}}\left[\left(1-\frac{\mu^2}{4}\right)\cos(\mu) - \frac{1}{2}\left(\frac{\mu}{-}+\mu\right)\sin(\mu)\right]. \tag{74}$$

The dispersion diagram classically displays band gaps as can be seen in Figure 3. We will now apply the high-frequency homogenisation technique to derive an analytical approximation to the higher branches of the diagram and to the associated wave fields.

In the case of a single eigenvalue, using (18), we find that $\hat{u}_0$ can be written as $\hat{u}_0 = A\cos(\mu_0 y) + B\sin(\mu_0 y)$ for some constants A and B, and, using Lemma 2.1, it is subject to the jump conditions

$$\begin{cases} \hat{u}_0(0^+) \mp \hat{u}_0(1^-) = \frac{1}{2}(\hat{u}_0'(0^+) \pm \hat{u}_0'(1^-)) \\ \hat{u}_0'(0^+) \mp \hat{u}_0'(1^-) = \frac{-\mu_0^2}{2}(\hat{u}_0(0^+) \pm \hat{u}_0(1^-)) \end{cases}, \tag{75}$$

where here and throughout the section, Notation 2.1 is being used. This leads to the relation

$$\mathcal{M}^{\mathrm{mo}}(A, B)^T = (0, 0)^T, \tag{76}$$

where the 2×2 matrix $\mathcal{M}^{\mathrm{mo}} = (\mathcal{M}^{\mathrm{mo}}_{ij})$ is given by

$$\mathcal{M}^{\mathrm{mo}} = \begin{pmatrix} 1 \mp \cos(\mu_0) \pm \frac{1}{2}\mu_0\sin(\mu_0) & \mp\sin(\mu_0) - \frac{\mu_0}{2}(1 \pm \cos(\mu_0)) \\ \mp\mu_0\sin(\mu_0) - \frac{\mu_0^2}{2}(1 \pm \cos(\mu_0)) & -\mu_0(1 \mp \cos(\mu_0)) \mp \frac{\mu_0^2}{2}\sin(\mu_0) \end{pmatrix}.$$

The only way for non-trivial solutions to (76) to exist is for its determinant to be zero, which after some algebraic manipulations, leads to a dispersion relation of the form

$$\mathcal{D}^{\mathrm{mo}}(\mu_0; ,) = 2(1 \mp \cos(\mu_0)) + \frac{}{2}\mu_0^2(1 \pm \cos(\mu_0)) \pm \mu_0\sin(\mu_0)\left(+\frac{1}{-}\right) = 0, \tag{77}$$

where the fact that $\mu_0 \neq 0$ has been used (we are not here interested in the low frequency limit). In practice, when calculating μ_0 and reconstructing $\hat{u}_0$, it can be useful to note that

$$\mathcal{M}^{\mathrm{mo}}_{22} = \frac{\pm\sin(\mu_0)}{1\pm\cos(\mu_0)}\mathcal{M}^{\mathrm{mo}}_{21},\ \mathcal{M}^{\mathrm{mo}}_{12} = \frac{1\pm\cos(\mu_0)}{\mp\sin(\mu_0)}\mathcal{M}^{\mathrm{mo}}_{11},\ \mathcal{M}^{\mathrm{mo}}_{11}\mathcal{M}^{\mathrm{mo}}_{21} = \mp\frac{\sin(\mu_0)}{2}\mathcal{D}^{\mathrm{mo}}(\mu_0; ,), \tag{78}$$

so that μ_0 is either a zero of $\mathcal{M}^{\text{mo}}_{11}$ or $\mathcal{M}^{\text{mo}}_{21}$, and in the former (resp. latter) case, the top (resp bottom) line of $\mathcal{M}^{\text{mo}}$ is zero (it can be shown that $\sin(\mu_0) \neq 0$). The computed eigenvalues are displayed on the dispersion diagram in Figure 3 (left) and, as expected, they coincide with the edges of the Brillouin zone. To obtain $\hat{u}_0$, we set $A = 1$, so that $\hat{u}_0(0^+) = 1$, and compute B using the first (resp. second) line in (76) if $\mathcal{M}^{\text{mo}}_{11} \neq 0$ (resp. $\mathcal{M}^{\text{mo}}_{21} \neq 0$).

Because we are ultimately interested in the value of T in (55), we need to calculate $\langle \beta w_1 \rangle$ in (49), and hence v_1 on the interval $(0, 1)$. We do this using the fact that it satisfies the same second-order equation (18a) as $\hat{u}_0$ and can hence be written $\mathrm{v}_1(y) = C\cos(\mu_0 y) + D\sin(\mu_0 y)$, for some constants C and D, which, using Remark 3.1, can be found by solving $\mathcal{M}^{\text{mo}}(C, D)^T = \boldsymbol{b}^{\text{mo}}$, where

$$\boldsymbol{b}^{\text{mo}} = \begin{pmatrix} \mp\hat{u}_0(1^-) \mp \frac{1}{2}\hat{u}_0'(1^-) \\ \mp\frac{\mu_0^2}{2}\hat{u}_0(1^-) \pm \hat{u}_0'(1^-) \end{pmatrix}. \tag{79}$$

Since $\mathcal{M}^{\text{mo}}$ is singular, (79) does not have a unique solution so we set $C = 1$ say and use the non-trivial line of the system to determine D. This works well since it can be shown that $\boldsymbol{b}^{\text{mo}}$ is such that $\boldsymbol{b}^{\text{mo}}_j = 0$ whenever $\mathcal{M}_{j,1} = 0$.

Once v_1 is found, the resulting value of T is directly obtained using (49). Note that, in this simple case, no numerical integration is required and calculations can be performed analytically. The resulting second-order approximations $\mu \approx \mu_0 + \frac{T}{2\mu_0}(\kappa\delta)^2$ and $\mu \approx \mu_0 + \frac{T}{2\mu_0}(\pi - \kappa\delta)^2$ (in the FFLW and FFFW cases respectively) are superposed to the dispersion diagram in Figure 3 (right), and one can see that they approximate the branches well in the vicinity of the edges of the Brillouin zone. One should also note that, as seen in Figure 4, this approximation remains valid within the band gaps, where $\kappa\delta$ is complex and is such that $\mathrm{Re}(\kappa\delta) = 0$ (FFLW) or $\mathrm{Re}(\kappa\delta) = \pi$ (FFFW). This is expected since in these cases, $(\kappa\delta)^2$ and $(\pi - \kappa\delta)^2$ remain real.

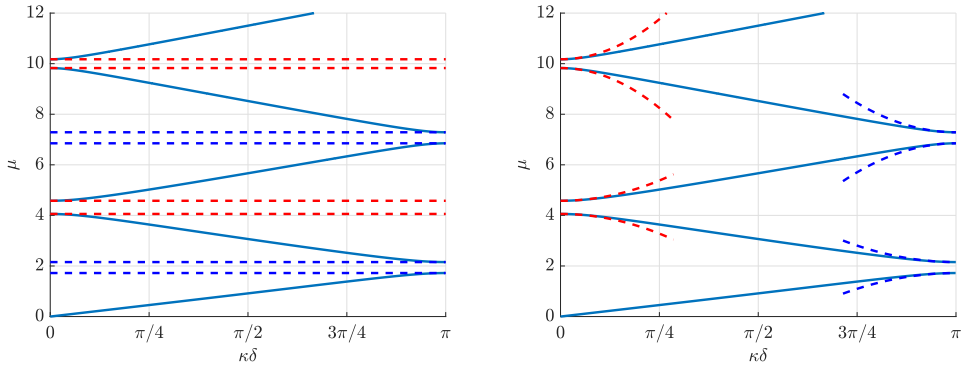

Figure 3: Dispersion diagram for the monolayer with = 1 and = 0.5. (Left) In red (resp. blue) dashed lines are the periodic (resp. antiperiodic) eigenvalues μ_0 calculated by finding the roots of (77). (Right) In red (resp. blue) dashed line are the periodic (resp. antiperiodic) resulting second-order approximations (55) using the computed values of T.

In Figure 5, we plot the zeroth-order approximation field $u_0(x, y) = u_0(\delta y, y) = \mathcal{U}_0(\delta y)\hat{u}_0(y)$ within three unit cells for the first four eigenvalues μ_0 in the FFLW and FFFW case for $\kappa\delta = \frac{\pi}{8}$ and $\kappa\delta = \frac{7\pi}{8}$ respectively. Here we have normalised $\hat{u}_0$ such that $\max_{(0,1)}|\hat{u}_0(y)| = 1$.

It appears that for the $2n$th eigenvalues ($n \in \mathbb{N}$), the wave field is actually continuous. This can be shown directly by realising that for these eigenvalues, this is the second line of $\mathcal{M}^{\text{mo}}$ that

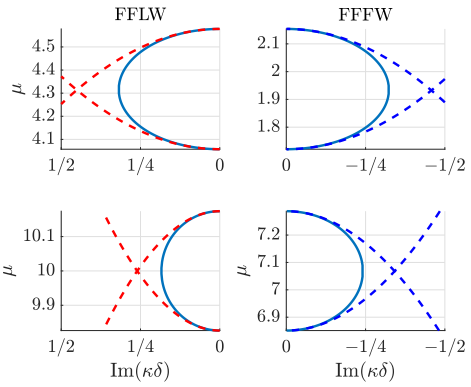

Figure 4: Imaginary part of $\kappa\delta$ in the band gaps of the monolayer dispersion diagram for $\quad = 1$ and $\quad = 0.5$. In red (resp. blue) dashed lines are the periodic (resp. antiperiodic) resulting second-order approximations (55) using the computed values of T, see also Figure 3 (right).

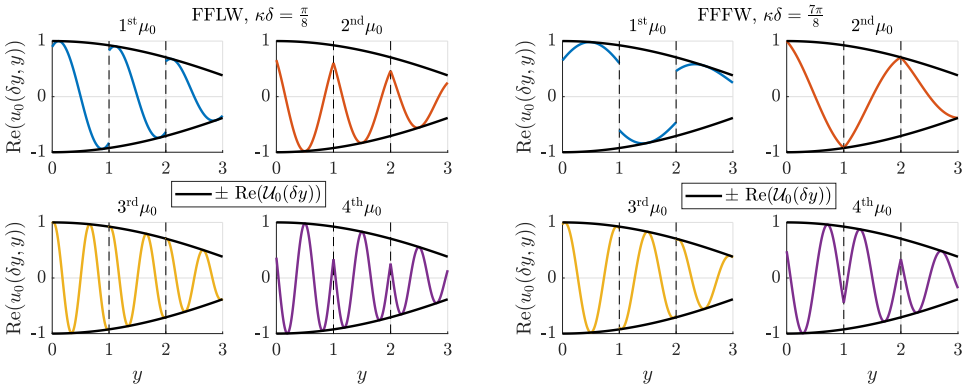

Figure 5: Real part of the zeroth-order approximation field $u_0(\delta y, y)$ corresponding the first four eigenvalues μ_0 along three unit cells with $\quad = 1$ and $\quad = 0.5$. A dashed vertical line represents the boundary between two adjacent unit cells. (Left) FFLW, $\kappa\delta = \frac{\pi}{8}\cdot$ (Right) FFFW, $\kappa\delta = \frac{7\pi}{8}\cdot$

is zero, and a little algebra hence shows that $\hat{u}_0(0^+) = \hat{u}_0(1^-)$ in this case.

Using the Bloch-Floquet analysis (see Appendix A), we can have access to the exact standing wave field $u_\delta(x) = u_\delta(\delta y)$, and, to be compatible with the asymptotic expansion (11), we normalise it such that $u_\delta(0^+) = u_0(0, 0^+)$. Note that because of (9) and (58), the difference between the exact and approximated field can be written as

$$u_\delta(x) - u_0\left(x, \frac{x}{\delta}\right) = u_\delta(\delta y) - u_0(\delta y, y) = \begin{cases} e^{i\kappa\delta y}(\mathfrak{u}_\delta(\delta y) - \hat{u}_0(y)) & \text{(FFLW)}, \\ e^{i\kappa\delta y}(\mathfrak{u}_\delta(\delta y) - e^{-i\pi y}\hat{u}_0(y)) & \text{(FFFW)}. \end{cases} \tag{80}$$

To illustrate the validity of our approximation, we hence compare $\mathfrak{u}_\delta(\delta y)$ and $\hat{u}_0(y)$ for various values of $\kappa\delta$ in Figure 6.

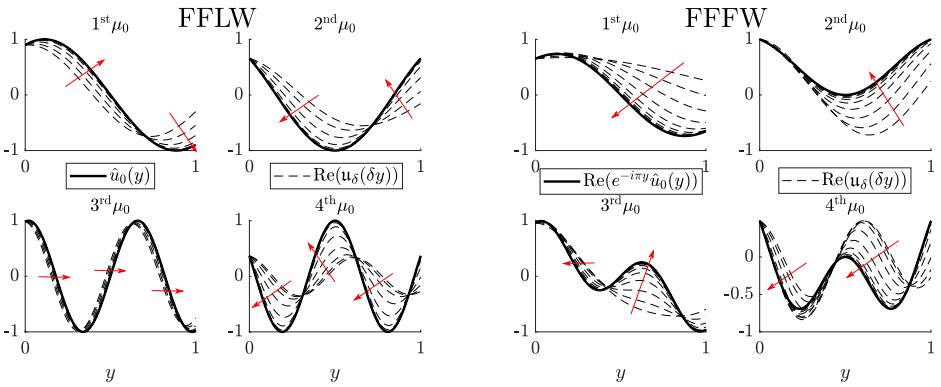

Figure 6: Illustration of the convergence of the method by comparing $\hat{u}_0$ and $\mathfrak{u}_\delta(\delta y)$ in the FFLW (left) and the FFFW (right) cases. We plotted $\mathfrak{u}_\delta$ for 20 values of $k\delta$ (FFLW) or $\pi - \kappa\delta$ (FFFW) equidistributed in the log scale between 10^{-5} and 1. The red arrows indicate how $\mathfrak{u}_\delta(\delta y)$ is changing as $\kappa\delta \to 0$ (FFLW) or $(\pi - \kappa\delta) \to 0$ (FFFW).

In Figure 7, we plot the error between the exact field and the homogenised field. Due to the periodicity properties of $\mathfrak{u}_\delta$ and $\hat{u}_0$ and (80), the error is relatively easy to compute and defined as follows:

$$\text{(FFLW error): } \mathcal{E}^{\text{FFLW}} = \max_{\mathbb{R}} |u_\delta(\delta y) - u_0(\delta y, y)| = \max_{(0,1)} |\mathfrak{u}_\delta(\delta y) - \hat{u}_0(y)|, \tag{81}$$

$$\text{(FFFW error): } \mathcal{E}^{\text{FFFW}} = \max_{\mathbb{R}} |u_\delta(\delta y) - u_0(\delta y, y)| = \max_{(0,1)} |\mathfrak{u}_\delta(\delta y) - e^{-i\pi y}\hat{u}_0(y)|. \tag{82}$$

One can see that we recover the expected behaviour $u_\delta(\delta y) = u_0(\delta y, y) + O(\kappa\delta)$ in the FFFW case and $u_\delta(\delta y) = u_0(\delta y, y) + O(\pi - \kappa\delta)$ in the FFLW case.

We now endeavour to study how the eigenvalues μ_0 depend on and . In order to visualise this we display a heat map of the first and second FFLW (periodic) $\mu_0(,)$ in Figure 8. One can clearly see two distinct regions, on the left and on the right of the curve = 1/. On each side of these curves, the eigenvalue depend solely on one of the two parameters (,), which correspond to either the top or the bottom line of $\mathcal{M}^{\text{mo}}$ being zero. On the curve = 1/, both lines of $\mathcal{M}^{\text{mo}}$ are zero, and hence, the eigenvalue μ_0 is a double eigenvalue.

The other eigenvalues in the the FFLW (periodic) and FFFW (antiperiodic) case have very similar heatmaps, in particular they are all double eigenvalues when = 1/, as displayed on the dispersion diagram in Figure 9 (left).

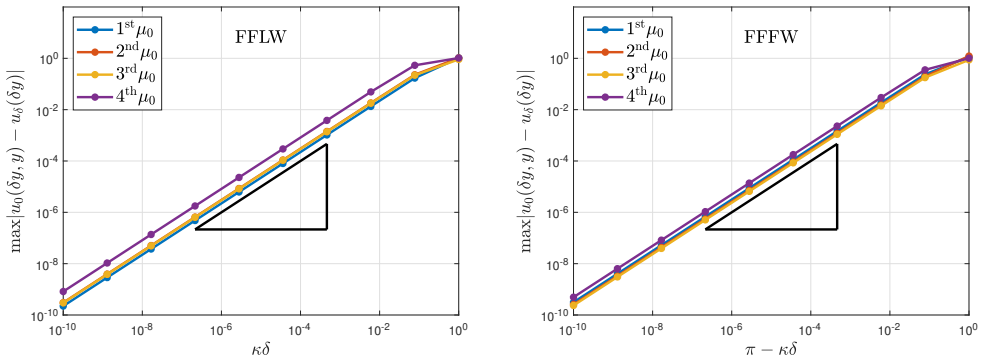

Figure 7: Loglog plot of the error between the exact (Bloch Floquet) and the homogenised fields for various values of $\kappa\delta$ with = 1 and = 0.5. (Left) FFLW. (Right) FFFW. The slope depicted by a black triangle denotes a $O(\kappa\delta)$ (FFLW) or a $O(\pi - \kappa\delta)$ (FFFW).

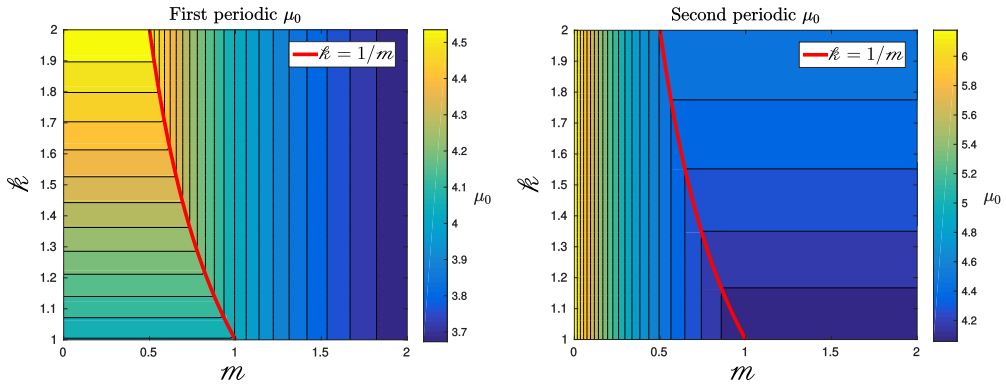

Figure 8: Filled contour plot of the first (left) and second (right) periodic eigenvalues μ_0 as and vary. The thick red line represents the locus of double eigenvalues, while the thin black lines are isolines of μ_0.

In the case of a double eigenvalue, we have to follow the procedure of §4 by representing u_0 as in (59). We hence need to find two independent solutions $\hat{u}_0^{(1,2)}$ of (18), which can both be written $\hat{u}_0^{(1,2)}(y) = A^{(1,2)}\cos(\mu_0 y) + B^{(1,2)}\sin(\mu_0 y)$. Because of the dimension of the system, any two independent vectors $(A^{(1)}, B^{(1)})^T$ and $(A^{(2)}, B^{(2)})^T$ would work, and we can hence choose $(A^{(1)}, B^{(1)})^T = (1,0)^T$ and $(A^{(2)}, B^{(2)})^T = (0,1)^T$. As seen in §4, the two functions $\boldsymbol{\mathcal{U}}_0^{(1,2)}(x)$ appearing in (59) satisfy the first-order ODE system (68), where in our case we have

$$B_1 = \langle\!\langle \hat{u}_0^{(1)} \rangle\!\rangle = \frac{1 \pm \cos(\mu_0)}{2},\ B_2 = \langle\!\langle \hat{u}_0^{(2)} \rangle\!\rangle = \frac{\pm \sin(\mu_0)}{2},\ C_1 = \langle \alpha (\hat{u}_0^{(1)})^2 \rangle = \frac{\mu_0 + \sin(\mu_0)\cos(\mu_0)}{2\mu_0},$$
$$D = \langle \alpha \hat{u}_0^{(1)} \hat{u}_0^{(2)} \rangle = \frac{\sin^2(\mu_0)}{2\mu_0},\ \langle \beta \mathtt{w}_0 \rangle = \mu_0,\ C_2 = \langle \alpha (\hat{u}_0^{(2)})^2 \rangle = \frac{\mu_0 - \sin(\mu_0)\cos(\mu_0)}{2\mu_0}.$$

Using these, one can easily compute the associated eigenvalues $\lambda_{1,2}$ and eigenvectors $\boldsymbol{\mathcal{U}}_{\lambda_{1,2}}$ via (69) and (70). Note that in this case, one can show that

$$B_1 B_2 + D = 0 \ \text{ and } \ B_1^2 + C_1 = B_2^2 + C_2,$$

so that the eigenvalues $\lambda_{1,2}$ and eigenvectors $\boldsymbol{\mathcal{U}}_{\lambda_{1,2}}$ of the matrix of the ODE system are simply

$$\lambda_j = i(-1)^j (B_1^2 + C_1) \ \text{ and } \ \boldsymbol{\mathcal{U}}_{\lambda_j} = (-i(-1)^j, 1)^T,$$

and $T_d = \mu_0/(B_1^2 + C_1)$. We can hence superpose the resulting linear approximation (73) onto the dispersion diagram, revealing an excellent fit, as can be seen in Figure 9 (right). It is quite remarkable that in this case, every eigenvalues μ_0 correspond to Dirac points. In fact this can be understood by considering a homogeneous material with only one spring-mass interface. Upon sending a wave onto this interface, one can naturally derive a coefficient of reflection $\mathrm{Ref}(\mu)$ and a coefficient of transmission $\mathrm{Trans}(\mu)$. It turns out that

$$\mathrm{Ref}(\mu) = \frac{-i\mu\left(\frac{1}{} - \right)}{2\left(1 - \frac{\mu^2}{4}\right) - i\mu\left(\frac{1}{} + \right)} \ \text{ and } \ \mathrm{Trans}(\mu) = \frac{2\left(1 + \frac{\mu^2}{4}\right)}{2\left(1 - \frac{\mu^2}{4}\right) - i\mu\left(\frac{1}{} + \right)},$$

and therefore the reflection coefficient is zero if and only if the condition $= 1/$ is satisfied. Hence, in the periodic medium considered, no internal reflection can be present, no destructive/constructive interference can take place and no band gaps occur.

5.2. Bilayer

We now consider the case of a bilayer material characterised by the phase fraction $r \in (0,1)$, and hence provide the imperfect interface extension to the example given in [6]. The unit cell is made up of two homogeneous materials. The first one has a length rh, density ρ_1 and Young's modulus E_1, while the second has length $(1-r)h$, density ρ_2 and Young's Modulus E_2. The two respective wave speeds are $c_1 = \sqrt{E_1/\rho_1}$ and $c_2 = \sqrt{E_2/\rho_2}$. The important non dimensional functions α and β are hence defined by

$$\alpha(y) = \begin{cases} \alpha^{(1)} = \rho_1/\rho^\star \ \text{ for } \ y \in (0,r), \\ \alpha^{(2)} = \rho_2/\rho^\star \ \text{ for } \ y \in (r,1), \end{cases} \ \text{ and } \ \beta(y) = \begin{cases} \beta^{(1)} = E_1/E^\star \ \text{ for } \ y \in (0,r), \\ \beta^{(2)} = E_2/E^\star \ \text{ for } \ y \in (r,1), \end{cases} \tag{83}$$

where $\rho^\star = r\rho_1 + (1-r)\rho_2$ and $E^\star = (r/E_1 + (1-r)/E_2)^{-1}$. The interface at $y = r$ is assumed perfect, and the geometry of this physical problem is summarised in Figure 10.

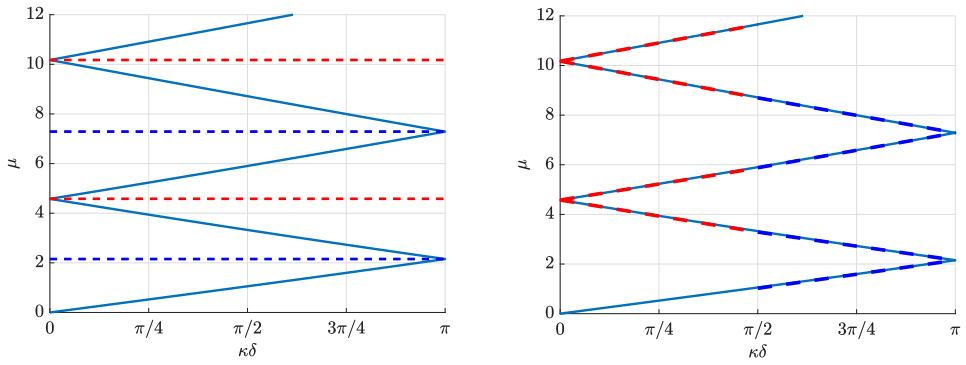

Figure 9: Dispersion diagram for the monolayer with = 2 and = 0.5 corresponding to double eigenvalues. (Left) In red (resp. blue) dashed lines are the periodic (resp. antiperiodic) eigenvalues μ_0 calculated by finding the roots of (77). (Right) In red (resp. blue) dashed line are the periodic (resp. antiperiodic) resulting first-order approximations (73).

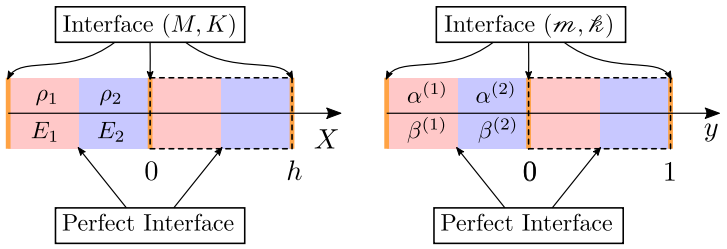

Figure 10: Geometry of the bilayer problem (left) and non-dimensional (right) settings.

The classic Bloch-Floquet analysis will, in this case, give the following dispersion relation

$$\cos(\kappa\delta) = \frac{1}{1+\frac{\mu^2}{4}}\left[\left(1-\frac{\mu^2}{4}\right)\left(C_1C_2 - \frac{1}{2}\left(\frac{Z_1}{Z_2}+\frac{Z_2}{Z_1}\right)S_1S_2\right)\right.$$
$$\left. - \frac{\mu}{2}\left(\frac{S_1C_2Z^\star}{Z_1}+\frac{S_2C_1Z^\star}{Z_2}\right) - \frac{\mu}{2}\left(\frac{Z_1S_1C_2}{Z^\star}+\frac{Z_2S_2C_1}{Z^\star}\right)\right], \tag{84}$$

where $Z^\star = \rho^\star c^\star$, and $C_i = \cos(\mu H_i)$, $S_i = \sin(\mu H_i)$, $H_1 = rc^\star/c_1$, $H_2 = (1-r)c^\star/c_2$ and, naturally, $c^\star = \sqrt{E^\star/\rho^\star}$. As per the monolayer case, the dispersion diagram displays band gaps as can be seen in Figure 11. We will now apply the high-frequency homogenisation technique to derive an analytical approximation to the higher branches of the diagram and to the associated wave fields.

Using (18a) and (19), we find that $\hat{u}_0$ should satisfy

$$\begin{cases} \hat{u}_0'' + (\Omega^{(1)})^2\hat{u}_0 = 0 \ \text{ on } \ (0,r), \\ \hat{u}_0'' + (\Omega^{(2)})^2\hat{u}_0 = 0 \ \text{ on } \ (r,1), \end{cases} \quad \text{so that} \quad \begin{cases} \hat{u}_0(y) = A^{(1)}\cos(\Omega^{(1)}y) + B^{(1)}\sin(\Omega^{(1)}y) \ \text{ on } \ (0,r), \\ \hat{u}_0(y) = A^{(2)}\cos(\Omega^{(2)}y) + B^{(2)}\sin(\Omega^{(2)}y) \ \text{ on } \ (r,1), \end{cases} \tag{85}$$

where $A^{(1,2)}$ and $B^{(1,2)}$ are some constants to be determined, and $\Omega^{(1,2)} = \mu_0\sqrt{\frac{\alpha^{(1,2)}}{\beta^{(1,2)}}} = \mu_0\frac{c^\star}{c_{1,2}}$. The interface at $y = r$ is assumed perfect, and hence, $\hat{u}_0$ is also subject to the interface conditions

$$\begin{cases} \hat{u}_0(r^-) = \hat{u}_0(r^+), \\ \beta^{(1)}\hat{u}_0'(r^-) = \beta^{(2)}\hat{u}_0'(r^+), \end{cases} \quad \text{and} \quad \begin{cases} \hat{u}_0(0^+) \mp \hat{u}_0(1^-) = \frac{1}{2}(\beta^{(1)}\hat{u}_0'(0^+) \pm \beta^{(2)}\hat{u}_0'(1^-)), \\ \beta^{(1)}\hat{u}_0'(0^+) \mp \beta^{(2)}\hat{u}_0'(1^-) = -\frac{\mu_0^2}{2}(\hat{u}_0(0^+) \pm \hat{u}_0(1^-)), \end{cases}$$

where here and throughout this section, Notation 2.1 is being used. This results in a system of the form

$$\mathcal{M}^{\text{bi}}(A^{(1)}, B^{(1)}, A^{(2)}, B^{(2)})^T = (0,0,0,0)^T, \tag{86}$$

where the 4×4 matrix $\mathcal{M}^{\text{bi}}$ is given by

$$\mathcal{M}^{\text{bi}} = \begin{pmatrix} 1 & -\frac{\beta^{(1)}\Omega^{(1)}}{2} & \mp\cos(\Omega^{(2)}) \pm \frac{\beta^{(2)}\Omega^{(2)}\sin(\Omega^{(2)})}{2} & \mp\sin(\Omega^{(2)}) \mp \frac{\beta^{(2)}\Omega^{(2)}\cos(\Omega^{(2)})}{2} \\ -\frac{\mu_0^2}{2} & -\beta^{(1)}\Omega^{(1)} & \mp\beta^{(2)}\Omega^{(2)}\sin(\Omega^{(2)}) \mp \frac{\mu_0^2}{2}\cos(\Omega^{(2)}) & \pm\beta^{(2)}\Omega^{(2)}\cos(\Omega^{(2)}) \mp \frac{\mu_0^2}{2}\sin(\Omega^{(2)}) \\ -\cos(\Omega^{(1)}r) & -\sin(\Omega^{(1)}r) & \cos(\Omega^{(2)}r) & \sin(\Omega^{(2)}r) \\ \beta^{(1)}\Omega^{(1)}\sin(\Omega^{(1)}r) & -\beta^{(1)}\Omega^{(1)}\cos(\Omega^{(1)}r) & -\beta^{(2)}\Omega^{(2)}\sin(\Omega^{(2)}r) & \beta^{(2)}\Omega^{(2)}\cos(\Omega^{(2)}r) \end{pmatrix}.$$

The equation (86) can only have non-trivial solutions if $\det(\mathcal{M}^{\text{bi}}) = 0$, which gives a relation of the form

$$\mathcal{D}^{\text{bi}}(\mu_0;,,\beta^{(1)},\beta^{(2)},\Omega^{(1)},\Omega^{(2)},r) = 0, \tag{87}$$

the roots of which correspond to the eigenvalues μ_0. The numerically computed eigenvalues are displayed on the dispersion diagram in Figure 11 (left), and, again, are shown to coincide with the edges of the Brillouin zone. To obtain $\hat{u}_0$, we find a vector in $\ker(\mathcal{M}^{\text{bi}})$ using the `null` function in Matlab, and use it as the coefficients $(A^{(1)}, B^{(1)}, A^{(2)}, B^{(2)})$.

We now need to find v_1 to obtain a second-order approximation. Since it is solution to the same equation (18a), we can write

$$\mathrm{v}_1(y) = \begin{cases} C^{(1)}\cos(\Omega^{(1)}y) + D^{(1)}\sin(\Omega^{(1)}y) \ \text{ on } \ (0,r), \\ C^{(2)}\cos(\Omega^{(2)}y) + D^{(2)}\sin(\Omega^{(2)}y) \ \text{ on } \ (r,1). \end{cases} \tag{88}$$

Using Remark 3.1 for the conditions at the unit cell interfaces, and remembering that, according to Remark 3.2, both v_1 and $\beta \mathrm{v}_1'$ should be continuous at $y = r$, one obtains a system of the form $\mathcal{M}^{\mathrm{bi}}(C^{(1)}, D^{(1)}, C^{(2)}, D^{(2)})^T = \boldsymbol{b}^{\mathrm{bi}}$, where

$$\boldsymbol{b}^{\mathrm{bi}} = \left(\mp \hat{u}_0(1^-) \mp \frac{1}{2}\beta^{(2)} \hat{u}_0'(1^-), \mp \frac{\mu_0^2}{2} \hat{u}_0(1^-) \pm \beta^{(2)} \hat{u}_0'(1^-), 0, 0 \right)^T .$$

Because the matrix $\mathcal{M}^{\mathrm{bi}}$ is singular, we compute $(C^{(1)}, D^{(1)}, C^{(2)}, D^{(2)})^T$ via the Moore-Penrose Pseudo-inverse [28]. Once v_1 is found, the resulting value of T is directly obtained using (49). The resulting approximations $\mu \approx \mu_0 + \frac{T}{2\mu_0}(\kappa\delta)^2$ and $\mu \approx \mu_0 + \frac{T}{2\mu_0}(\pi - \kappa\delta)^2$ (in the FFLW and FFFW cases respectively) are superposed to the Bloch-Floquet diagram in Figure 11 (right), and one can see that they approximate the branches well in the vicinity of the edges of the band gaps of the dispersion diagram. It is apparent from Figure 11 (left) that the highest antiperiodic eigenvalue displayed seems to be a double eigenvalue. This case and the resulting linear approximations will be discussed later.

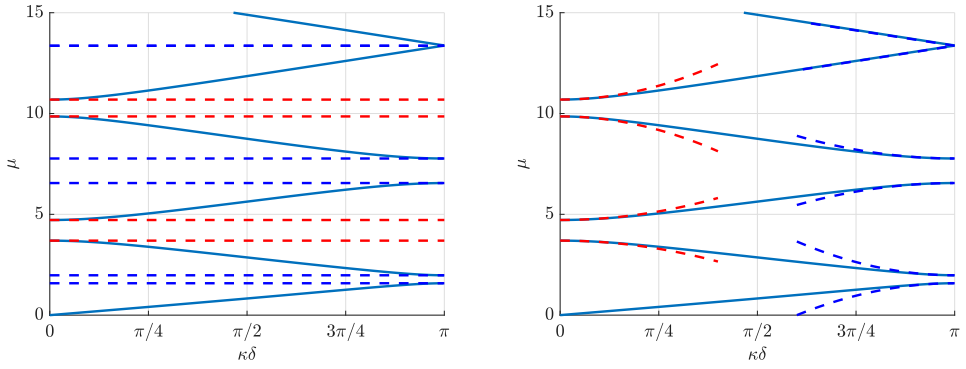

Figure 11: Non-dimensional dispersion diagram for the bilayer with $\rho_1 = 1200\,\mathrm{kg.m^{-3}}$, $\rho_2 = 1800\,\mathrm{kg.m^{-3}}$, $c_1 = 2800\mathrm{m.s^{-1}}$, $c_2 = 3500\,\mathrm{m.s^{-1}}$, $E_1 = \rho_1 c_1^2$, $E_2 = \rho_2 c_2^2$, $M = 2 \times 10^4\,\mathrm{kg.m^2}$, $K = 2.45 \times 10^9\,\mathrm{Pa.m^{-1}}$, $r = 0.202$ and $h = 10\,\mathrm{m}$, corresponding to ≈ 1.41 and ≈ 1.19, $\alpha^{(1)} \approx 0.71$, $\alpha^{(2)} \approx 1.071$, $\beta^{(1)} \approx 0.54$ and $\beta^{(2)} \approx 1.27$. (Left) The red (resp. blue) dashed lines are the periodic (resp. antiperiodic) eigenvalues μ_0 calculated by finding the roots of (77). (Right) The red (resp. blue) dashed lines are the periodic (resp. antiperiodic) resulting second-order approximations (55) using the computed values of T or in the case of the almost-Dirac point, the linear approximation (73).

In Figure 12, we plot the approximated field $u_0(x, y) = u_0(\delta y, y)$ within three unit cells for the first four μ_0 in the FFLW and FFFW case for $\kappa\delta = \frac{\pi}{8}$ and $\kappa\delta = \frac{7\pi}{8}$ respectively. Here we have normalised $\hat{u}_0$ such that $\max_{(0,1)} |\hat{u}_0(y)| = 1$.

Using the Bloch-Floquet analysis, in a very similar way to the monolayer case, we can have access to the exact standing wave field $u_\delta(x) = u_\delta(\delta y)$, and we normalise it such that $u_\delta(0^+) = u_0(0, 0^+)$. As per the monolayer case, and because of (80), we illustrate the convergence of the method by comparing $\mathfrak{u}_\delta(\delta y)$ and $\hat{u}_0(y)$ for various values of $\kappa\delta$ in Figure 13.

In Figure 14, we plot the error between the exact field and the homogenised field. This error can be expressed as in (81) and (82). Again, one can see that we recover the expected behaviour $u_\delta(\delta y) = u_0(\delta y, y) + O(\kappa\delta)$ in the FFFW case and $u_\delta(\delta y) = u_0(\delta y, y) + O(\pi - \kappa\delta)$ in the FFLW case.

As for the monolayer example displayed in Figure 9, it is possible to find physical parameters such that all the eigenvalues become simultaneously double eigenvalues (Dirac points). In order

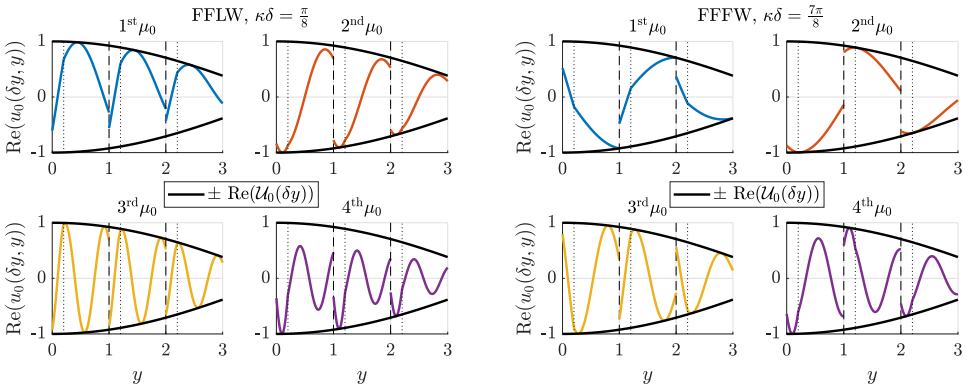

Figure 12: Real part of the field $u_0(\delta y, y)$ corresponding the first four eigenvalues μ_0 along three unit cells for the bilayer case for the same parameters used in Figure 11. A dashed vertical line represents a boundary between two adjacent unit cells, while a dotted vertical line represents the location of the perfect interface between the two homogeneous materials. (Left) FFLW, $\kappa\delta = \frac{\pi}{8}\cdot$ (Right) FFFW, $\kappa\delta = \frac{7\pi}{8}\cdot$

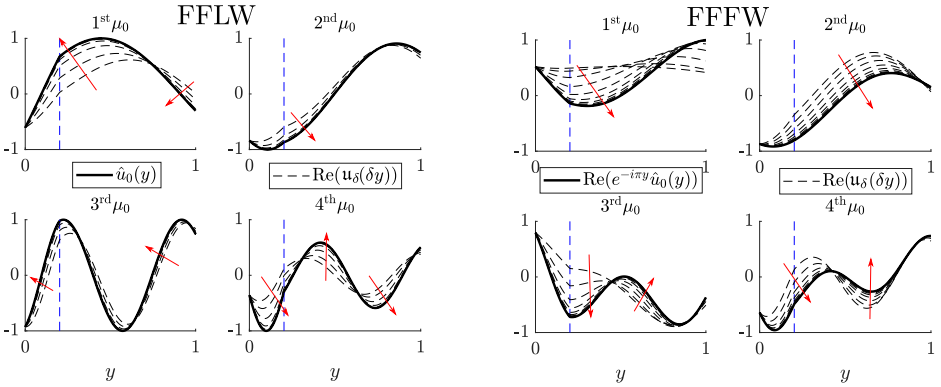

Figure 13: Illustration of the convergence of the method by comparing $\hat{u}_0$ and $\mathfrak{u}_\delta(\delta y)$ in the FFLW (left) and the FFFW (right) cases. We plotted $\mathfrak{u}_\delta$ for 20 values of $k\delta$ (FFLW) or $\pi - \kappa\delta$ (FFFW) equidistributed in the log scale between 10^{-5} and 1. The red arrows indicate how $\mathfrak{u}_\delta(\delta y)$ is changing as $\kappa\delta \to 0$ (FFLW) or $(\pi - \kappa\delta) \to 0$ (FFFW), while the vertical dashed blue line indicates the position of the perfect interface between the two homogeneous materials.

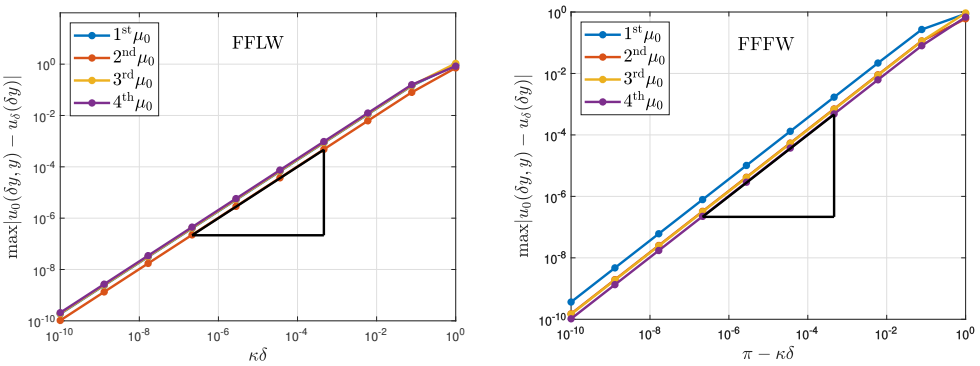

Figure 14: Loglog plot of the error between the exact (Bloch Floquet) and the homogenised fields for various values of $\kappa\delta$ and for the same parameters used in Figure 11. (Left) FFLW. (Right) FFFW. The slope depicted by a black triangle denotes a $O(\kappa\delta)$ (FFLW) or a $O(\pi - \kappa\delta)$ (FFFW).

to do so one needs to ensure that $= 1/$, and that $\rho_1 c_1 = \rho_2 c_2$. The first conditions imposes that the reflection coefficient due to the imperfect interface is zero, and the second imposes that the two homogeneous materials are "impedance matched" so that no reflection occurs from their perfect interface either.

However, in this case, it appears that certain parameters could lead to only two of the eigenvalues to merge into a double eigenvalue, as appears to be the case in Figure 11 (left). In order to visualise this phenomena, one could look at the evolution of the eigenvalues μ_0 for fixed physical parameter, but for varying r within $(0, 1)$. The results are displayed in Figure 15, and it seems that double eigenvalues or near-double eigenvalues may occur for some specific values of r, though, in this case, all the eigenvalues do not become double simultaneously. In fact, as illustrated in Figure 15, if one zooms on the areas of the graphs where eigenvalues seem to coincide, it appears that the curves do not actually touch each other. We will call these points *almost-Dirac points*. A linear approximation to the dispersion diagram near these almost-Dirac points can be obtained by following the procedure of §4, as can be seen in Figure 11 (right), though the details will not be reproduced here for brevity.

To explore the parameter space further, we will keep the values of r, $\alpha^{(1,2)}$ and $\beta^{(1,2)}$ used in Figure 11 and study the variation of the fifth and sixth antiperiodic eigenvalues μ_0 that correspond to an almost-Dirac point according to Figure 15. As can be seen in Figure 16, in this case, we observe a similar behaviour as that of Figure 8, where two distinct regions seem to be separated by a smooth curve, on which the values of and chosen in Figure 11 (represented by a black star) seem to lie.

All in all, it seems to be the case, that for a given integer j, the j^{th} eigenvalue is double on some manifold given by $\mathfrak{F}_j(\rho_1, \rho_2, E_1, E_2, M, K, r) = 0$ for some function $\mathfrak{F}_j$, though finding an analytical expression for $\mathfrak{F}_j$ is beyond the scope of the present work.

6. Conclusion

In this work, we have extended the technique of high-order homogenisation to one-dimensional periodic media with linear imperfect interfaces of the spring-mass type. The extension was not

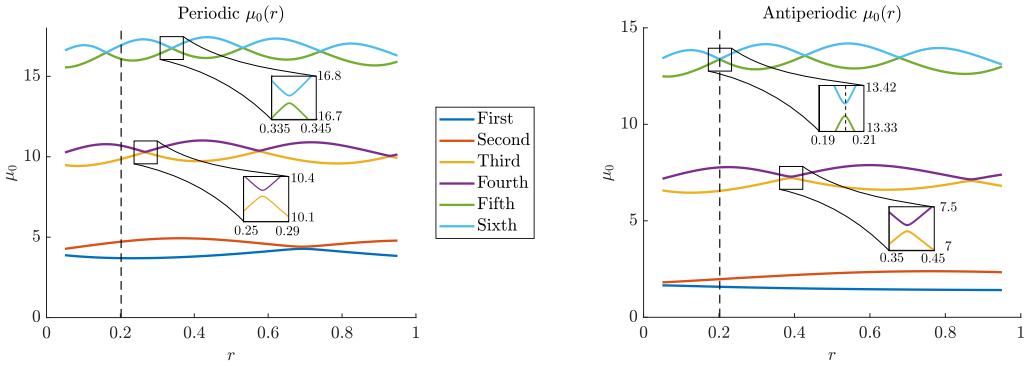

Figure 15: Evolution of the first six FFLW (left) and FFFW (right) eigenvalues μ_0 for the exact same parameters as those used in Figure 11, but for $r \in (0.05, 0.95)$. A vertical dashed line represents the value of r used in Figure 11. Zoom boxes are provided to show that near the almost-Dirac points, the eigenvalues remain simple.

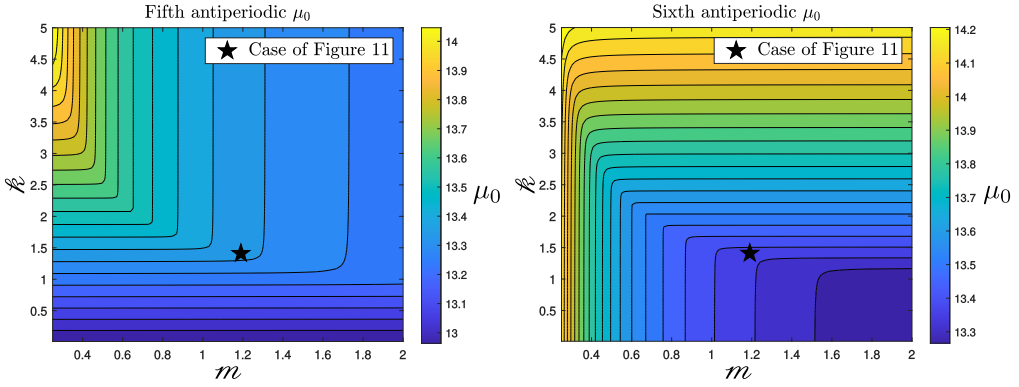

Figure 16: Filled Contour Plot of the variations of the fifth (left) and sixth (right) antiperiodic eigenvalues in the bilayer case for the same values of r, $\alpha^{(1,2)}$ and $\beta^{(1,2)}$ used in Figure 11. The black star corresponds to the values of and used in Figure 11.

direct, and many of the proofs for the classic case needed to be extended in order to deal with the extra technical difficulties arising from imperfect interface. We have also described how the technique should be modified in the specific case of Dirac points within the dispersion diagram. We have illustrated the validity of our theoretical development with the two examples of monolayered and bilayered materials. In the case of the monolayered material, we quantified the error between the exact and the homogenised field, and we found a simple condition on the nondimensional stiffness and mass values and for all the points at the edges of the Brillouin zone to become Dirac points. Similar conditions were given in the bilayered case. Moreover, in the bilayered case, almost-Dirac points have been identified while exploring the parameter space (much larger than that of the monolayered material). As mentioned previously, one of the advantages of high-frequency homogenisation is that it works even when the dispersion diagrams cannot be obtained analytically or are computationally intricate to obtain. In such cases, this high-frequency homogenisation approach may, for example, provide a way of back-engineering the values of and describing imperfect interface, or pick specific material properties and contact in order to ensure the presence of Dirac points, which are known to display very interesting physical properties.

Appendix A. Bloch-Floquet analysis of the monolayer case

In this case, u_δ satisfies (7) with $\alpha \equiv \beta \equiv 1$, hence, on $(0,\delta)$, we have

$$u_\delta(x) = A_{\rm BF}\cos\left(\frac{\mu x}{\delta}\right) + B_{\rm BF}\sin\left(\frac{\mu x}{\delta}\right), \tag{A.1}$$

$$u'_\delta(x) = -\frac{A_{\rm BF}\mu}{\delta}\sin\left(\frac{\mu x}{\delta}\right) + \frac{B_{\rm BF}\mu}{\delta}\cos\left(\frac{\mu x}{\delta}\right), \tag{A.2}$$

subject to the two jump conditions $[\![u_\delta]\!]_0 = \frac{\delta}{}\langle\!\langle u'_\delta\rangle\!\rangle_0$ and $\delta[\![u'_\delta]\!]_0 = -\mu^2\langle\!\langle u_\delta\rangle\!\rangle_0$, relating the value of u_δ and u'_δ at 0^+ and 0^-. Moreover, according to Bloch-Floquet theory, we know that we can write $u_\delta(x) = \mathfrak{u}_\delta(x)e^{i\kappa x}$, for a δ-periodic function $\mathfrak{u}_\delta$, implying that, in particular, we have $u_\delta(\delta^-) = u_\delta(0^-)e^{i\kappa\delta}$ and $u'_\delta(\delta^-) = u'_\delta(0^-)e^{i\kappa\delta}$. This, combined with the jump conditions, relates the values of u_δ and u'_δ at 0^+ and δ^-, and hence it gives two equations on $A_{\rm BF}$ and $B_{\rm BF}$. These equations can be summarised by a matrix equation of the form $\mathcal{M}^{\rm mo}_{\rm BF}(\mu,\kappa\delta,,)(A_{\rm BF},B_{\rm BF})^T = (0,0)^T$, where

$$\mathcal{M}^{\rm mo}_{\rm BF} = \begin{pmatrix} 1 - e^{-i\kappa\delta}\cos(\mu) + \frac{\mu}{2}\sin(\mu)e^{-i\kappa\delta} & -\sin(\mu)e^{-i\kappa\delta} - \frac{\mu}{2}(1+\cos(\mu)e^{-i\kappa\delta}) \\ -\mu\sin(\mu)e^{-i\kappa\delta} - \frac{\mu^2}{2}(1+\cos(\mu)e^{-i\kappa\delta}) & -\mu(1-\cos(\mu)e^{-i\kappa\delta}) - \frac{\mu^2}{2}\sin(\mu)e^{-i\kappa\delta} \end{pmatrix}.$$

One notes that, as expected, for $\kappa\delta = 0$ or $\kappa\delta = \pi$ we have $\mathcal{M}^{\rm mo}_{\rm BF} = \mathcal{M}^{\rm mo}$ with the relevant sign. Of course, this system has only non-trivial solutions if $\det(\mathcal{M}^{\rm mo}_{\rm BF}) = 0$. A little bit of algebra shows that

$$\det(\mathcal{M}^{\rm mo}_{\rm BF}) = \mu\left(-\mathcal{B} + 2e^{-i\kappa\delta}\left(C\cos(\mu) - \frac{1}{2}\left(\frac{1}{-}+\right)\mu\sin(\mu)\right) - \mathcal{B}e^{-2i\kappa\delta}\right),$$

where $\mathcal{B} = 1 + \frac{\mu^2}{4}$ and $C = 1 - \frac{\mu^2}{4}$. Equating it to zero and multiplying by $e^{i\kappa\delta}/(\mathcal{B}\mu)$, this leads to the dispersion relation (74). For a value of μ satisfying the dispersion relation, we have infinitely many possible $(A_{\rm BF},B_{\rm BF})^T$. To find one, just fix $A_{\rm BF} = 1$, and use either the first or second line of $\mathcal{M}^{\rm mo}_{\rm BF}$ to get $B_{\rm BF}$ as follows:

$$B_{\rm BF} = \frac{1 + e^{-i\kappa\delta}\left(-\cos(\mu) + \frac{\mu}{2}\sin(\mu)\right)}{\frac{\mu}{2} + e^{-i\kappa\delta}\left(\sin(\mu) + \frac{\mu}{2}\cos(\mu)\right)} \quad \text{or} \quad B_{\rm BF} = \frac{\frac{\mu}{2} + e^{-i\kappa\delta}\left(\sin(\mu) + \frac{\mu}{2}\cos(\mu)\right)}{-1 + e^{-i\kappa\delta}\left(\cos(\mu) - \frac{\mu}{2}\sin(\mu)\right)},$$

depending on which one has a non-zero denominator. It then leads to the exact Bloch-Floquet solution $u_\delta(x)$ on $(0, \delta)$. From this we recover $\mathfrak{u}_\delta(x) = u_\delta(x)e^{-i\kappa x}$ on $(0, \delta)$, which we can extend to $x \in \mathbb{R}$ by periodicity. We can therefore get $u_\delta(x)$ everywhere by $u_\delta(x) = \mathfrak{u}_\delta(x)e^{i\kappa x}$.

[1] A. Bensoussan, J.-L. Lions, G. Papanicolaou, Asymptotic analysis for periodic structures, North-Holland, 1978.

[2] N. Bakhvalov, G. Panasenko, Homogenisation: averaging process in periodic media, Kluwer Academic Publishers, 1984.

[3] D. Cioranescu, P. Donato, An Introduction to Homogenization. Oxford lecture series in mathematics and its applications, Vol. 17, OUP, 1999. doi:10.14708/ma.v28i42/01.1882.

[4] V. Laude, Phononic Crystals: Artificial Crystals for Sonic, Acoustic, and Elastic Waves, De Gruyter, 2015.

[5] T. Gorishnyy, M. Maldovan, C. Ullal, E. Thomas, Sound ideas, Physics World 18 (12) (2005) 24–29. doi:10.1088/2058-7058/18/12/30.
URL https://doi.org/10.1088/2058-7058/18/12/30

[6] R. V. Craster, J. Kaplunov, A. V. Pichugin, High-frequency homogenization for periodic media, Proc. R. Soc. A 466 (2120) (2010) 2341–2362. doi:10.1098/rspa.2009.0612.

[7] B. B. Guzina, S. Meng, O. Oudghiri-Idrissi, A rational framework for dynamic homogenization at finite wavelengths and frequencies, Proc. R. Soc. A 475 (2223) (2019) 1–29. arXiv:1805.07496, doi:10.1098/rspa.2018.0547.

[8] S. Meng, O. Oudghiri-Idrissi, B. B. Guzina, A convergent low-wavenumber, high-frequency homogenization of the wave equation in periodic media with a source term, arXiv preprint 2002.028338v1 (2020) 1–25arXiv:2002.02838.
URL http://arxiv.org/abs/2002.02838

[9] D. Harutyunyan, G. W. Milton, R. V. Craster, High-frequency homogenization for travelling waves in periodic media, Proc. R. Soc. A 472 (2191) (2016) 20160066. doi:10.1098/rspa.2016.0066.
URL https://doi.org/10.1098/rspa.2016.0066

[10] E. Nolde, R. Craster, J. Kaplunov, High frequency homogenization for structural mechanics, J. Mech. Phys. Solids 59 (3) (2011) 651–671. doi:10.1016/j.jmps.2010.12.004.
URL https://doi.org/10.1016/j.jmps.2010.12.004

[11] D. J. Colquitt, R. V. Craster, M. Makwana, High frequency homogenisation for elastic lattices, Q. J. Mech. Appl. Math. 68 (2) (2015) 203–230. doi:10.1093/qjmam/hbv005.
URL https://doi.org/10.1093/qjmam/hbv005

[12] I. Sevostianov, R. Rodriguez-Ramos, R. Guinovart-Diaz, J. Bravo-Castillero, F. J. Sabina, Connections between different models describing imperfect interfaces in periodic fiber-reinforced composites, J. Mech. Solid. Struct. 49 (13) (2012) 1518–1525. doi:10.1016/j.ijsolstr.2012.02.028.
URL http://dx.doi.org/10.1016/j.ijsolstr.2012.02.028

[13] Y. C. Angel, J. D. Achenbach, Reflection of ultrasonic waves by an array of microcracks, in: D. Thompson, D. Chimenti (Eds.), Review of Progress in Quantitative Nondestructive Evaluation, Springer, 1985, pp. 83–89.

[14] A. Pilarski, J. L. Rose, A transverse-wave ultrasonic oblique-incidence technique for interfacial weakness detection in adhesive bonds, Journal of Applied Physics 63 (2) (1988) 300–307. doi:10.1063/1.340294.
URL https://doi.org/10.1063/1.340294

[15] A. Pilarski, J. L. Rose, K. Balasubramaniam, The angular and frequency characteristics of reflectivity from a solid layer embedded between two solids with imperfect boundary conditions, J. Acoust. Soc. Am. 87 (2) (1990) 532–542. doi:10.1121/1.398924.
URL https://doi.org/10.1121/1.398924

[16] M. Schoenberg, Elastic wave behavior across linear slip interfaces, J. Acoust. Soc. Am. 68 (5) (1980) 1516–1521. doi:10.1121/1.385077.
URL https://doi.org/10.1121/1.385077

[17] J.-M. Baik, R. B. Thompson, Ultrasonic scattering from imperfect interfaces: A quasi-static model, J. Nondestruct. Eval. 4 (3-4) (1984) 177–196. doi:10.1007/bf00566223.
URL https://doi.org/10.1007/bf00566223

[18] S. I. Rokhlin, Y. J. Wang, Analysis of boundary conditions for elastic wave interaction with an interface between two solids, J. Acoust. Soc. Am. 89 (2) (1991) 503–515. doi:10.1121/1.400374.
URL https://doi.org/10.1121/1.400374

[19] P. P. Delsanto, M. Scalerandi, A spring model for the simulation of the propagation of ultrasonic pulses through imperfect contact interfaces, J. Acoust. Soc. Am. 104 (5) (1998) 2584–2591. doi:10.1121/1.423841.
URL https://doi.org/10.1121/1.423841

[20] H. G. Tattersall, The ultrasonic pulse-echo technique as applied to adhesion testing, J. Phys. D 6 (7) (1973) 819–832. doi:10.1088/0022-3727/6/7/305.
URL https://doi.org/10.1088/0022-3727/6/7/305

[21] C. Licht, F. Lebon, A. Léger, Dynamics of elastic bodies connected by a thin adhesive layer, in: A. Leger, M. De-

schamps (Eds.), Ultrasonic Wave Propagation in Non Homogeneous Media, Vol. 128, Springer Proceedings in Physics, 2009, pp. 99–110.

[22] C. Bellis, M. Touboul, B. Lombard, R. C. Assier, Effective dynamics for transient elastic waves in a 1d periodic array of nonlinear interfaces, To be submitted.

[23] Z. Hashin, Thermoelastic properties of fiber composites with imperfect interface, Mechanics of Materials 8 (1990) 333–348.

[24] Z. Hashin, Thin interphase/imperfect interface in elasticity with application to coated fiber composites, J. Mech. Phys. Solids 50 (12) (2002) 2509–2537. doi:10.1016/S0022-5096(02)00050-9.

[25] J. C. López-Realpozo, R. Rodríguez-Ramos, R. Guinovart-Díaz, J. Bravo-Castillero, L. P. Fernández, F. J. Sabina, G. A. Maugin, Effective properties of non-linear elastic laminated composites with perfect and imperfect contact conditions, Mech. Adv. Mater. Struc. 15 (5) (2008) 375–385. doi:10.1080/15376490801977742.

[26] J. P. Lee-Thorp, M. I. Weinstein, Y. Zhu, Elliptic operators with honeycomb symmetry: Dirac points, edge states and applications to photonic graphene, Arch. Ration. Mech. Anal. 232 (1) (2018) 1–63. doi:10.1007/s00205-018-1315-4.
URL https://doi.org/10.1007/s00205-018-1315-4

[27] T. Ochiai, M. Onoda, Photonic analog of graphene model and its extension: Dirac cone, symmetry, and edge states, Phys. Rev. B 80 (15). doi:10.1103/physrevb.80.155103.
URL https://doi.org/10.1103/physrevb.80.155103

[28] R. Penrose, A generalized inverse for matrices, Math. Proc. Cambridge 51 (3) (1955) 406–413. doi:10.1017/s0305004100030401.
URL https://doi.org/10.1017/s0305004100030401